Variable Stars in the Unusual, Metal-Rich Globular Cluster NGC 6388

Barton J. Pritzl[1,2] and Horace A. Smith

Dept. of Physics and Astronomy, Michigan State University, East Lansing, MI 48824

e-mail: pritzl@pa.msu.edu, smith@pa.msu.edu

Márcio Catelan

Pontificia Universidad Católica de Chile, Departamento de Astronomía y Astrofísica, Av. Vicuña Mackenna 4860, 6904411 Macul, Santiago, Chile

email: mcatelan@astro.puc.cl

and

Allen V. Sweigart

NASA Goddard Space Flight Center, Laboratory for Astronomy and Solar Physics, Code 681, Greenbelt, MD 20771

e-mail: sweigart@bach.gsfc.nasa.gov

Received _____ _____; accepted _____

Draft, 02/26/02 - v6.1

---

[1]Visiting Astronomer, Cerro Tololo Inter-American Observatory, National Optical Astronomy Observatories, which is operated by AURA, Inc., under cooperative agreement with the National Science Foundation.

[2]Current address: National Optical Astronomy Observatories, P.O. Box 26732, Tucson, AZ 85726, email: pritzl@noao.edu

ABSTRACT

We have undertaken a search for variable stars in the metal-rich globular cluster NGC 6388 using time-series BV photometry. Twenty-eight new variables were found in this survey, increasing the total number of variables found near NGC 6388 to ~ 57. A significant number of the variables are RR Lyrae (~ 14), most of which are probable cluster members. The periods of the fundamental mode RR Lyrae are shown to be unusually long compared to metal-rich field stars. The existence of these long period RRab stars suggests that the horizontal branch of NGC 6388 is unusually bright. This implies that the metallicity-luminosity relationship for RR Lyrae stars is not universal if the RR Lyrae in NGC 6388 are indeed metal-rich. We consider the alternative possibility that the stars in NGC 6388 may span a range in [Fe/H]. Four candidate Population II Cepheids were also found. If they are members of the cluster, NGC 6388 would be the most metal-rich globular cluster to contain Population II Cepheids. The mean V magnitude of the RR Lyrae is found to be 16.85 ± 0.05 resulting in a distance of 9.0 to 10.3 kpc, for a range of assumed values of $\langle M_V \rangle$ for RR Lyrae. We determine the reddening of the cluster to be $E(B-V) = 0.40 \pm 0.03$ mag, with differential reddening across the face of the cluster. We discuss the difficulty in determining the Oosterhoff classification of NGC 6388 and NGC 6441 due to the unusual nature of their RR Lyrae, and address evolutionary constraints on a recent suggestion that they are of Oosterhoff type II.

Subject headings: Stars: variables: RR Lyrae stars; Galaxy: globular cluster: individual (NGC 6388)

1. Introduction

NGC 6388, at [Fe/H] $= -0.60 \pm 0.15$ (Armandroff & Zinn 1988), is slightly more metal-rich than 47 Tucanae (NGC 104). One would therefore expect that the color-magnitude diagram (CMD) of NGC 6388 would show a stubby red horizontal branch (HB) characteristic of metal-rich globular clusters such as 47 Tuc. Alcaino (1981) found that NGC 6388 contains a strong, red HB component in addition to a small number of stars blueward of the red HB. Hazen & Hesser (1986) discovered a number of variables within the tidal radius of NGC 6388 in addition to those previously found (Lloyd Evans & Menzies 1973, 1977). They found that as many as 6 of these variables were RR Lyrae (RRL) and were likely cluster members. At the time, this made NGC 6388 the most metal-rich globular cluster known to contain RRL. In a more recent study, Silbermann et al. (1994) presented (V, $B-V$) and (V, $V-R$) CMDs which confirmed Alcaino's previous finding that NGC 6388 contains a weak blue HB component. An additional 3 RRL were found in their survey along with 4 suspected variables. Unfortunately, their data were obtained under seeing conditions not favorable for observing variable stars in such a crowded environment.

Rich et al. (1997), using *Hubble Space Telescope* (HST) observations, discovered that the CMD of NGC 6388 actually has a pronounced blue HB component, which stretches across the location of the instability strip. The presence of hot HB stars in NGC 6388 was originally suggested by Rich, Minniti, & Liebert (1993) on the basis of integrated-light observations in the UV. Not only does the HB have a blue component, but it also slopes upward as one goes blueward in a (V, $B-V$) CMD. NGC 6388 is not, however, unique in these characteristics: As we noted in Pritzl et al. (2001; hereafter Paper I), Rich et al. showed that the CMD of the relatively metal-rich globular cluster NGC 6441 has a similar HB morphology. It has long been known that the HB morphology of globular clusters does not correlate perfectly with [Fe/H] and that at least one parameter besides [Fe/H] is

needed to account for this (Sandage & Wildey 1967; van den Bergh 1967). NGC 6441 and NGC 6388 are the only metal-rich globular clusters known to exhibit this second parameter effect. Very recently, the presence of a blue HB component was suggested also for the metal-rich globular cluster Terzan 5 (Cohn et al. 2002), a cluster which has also been found to contain a long-period RRL (Edmonds et al. 2001).

A number of possible explanations for the unusual nature of the HBs in NGC 6388 and NGC 6441 have been proposed (Sweigart & Catelan 1998; Sweigart 1999, 2002; Paper I; Raimondo et al. 2002). Several of these theoretical explanations predict that the HBs in these clusters are unusually bright, which would imply unusually long periods for their RRLs. It has already been shown that NGC 6441 contains a number of RRL with unusually long periods (Layden et al. 1999; Paper I).

In this paper we report new B and V photometry of NGC 6388 which has led to the discovery of additional variable stars. Preliminary results from these observations have already been used to argue that the RRLs in NGC 6388 are unusually bright for the cluster metallicity (Pritzl et al. 2000). Here we present the results of the new study in detail and call attention to several unusual properties of RRLs in NGC 6388 while noting the similarities and differences to NGC 6441.

2. Observations and Reductions

NGC 6388 was observed in conjunction with NGC 6441 (see Paper I for detailed discussion on the observations and reductions). Time series observations of NGC 6388 were obtained at the 0.9 m telescope at Cerro Tololo Inter-American Observatory (CTIO) using the Tek 2K No. 3 CCD detector with a field size of 13.5 arcmin per side. Time series observations of NGC 6388 were obtained on the UT dates of May 26, 27, 28, and 29, and

June 1, 2, 3, and 4, 1998. Exposures of 600 seconds were obtained in both B and V filters. The seeing ranged from 1.1 to 2.5 arcsec, with a typical seeing of 1.4 arcsec.

Landolt (1992) and Graham (1982) standard stars were observed on June 1, 2, and 3. These primary standard stars spanned a color range from $B-V = 0.024$ to 2.326 mag, adequate to cover the color range of the reddened stars in NGC 6388. Primary standards were observed between airmasses 1.035 and 1.392. Only the night of June 1 was photometric, but standards observed on the nonphotometric nights were incorporated in the reductions using the "cloudy" night reduction routines created by Peter Stetson (private communications).

Instrumental magnitudes v and b for the NGC 6388 stars were transformed to Johnson V and B magnitudes using Stetson's TRIAL package. 71 local standards within the NGC 6388 field were used to set the frame-by-frame zero-points for the cluster observations. Because NGC 6388 was observed to higher airmass than the Landolt (1992) and Graham (1982) standards, the local standards were also used to check the adopted values of the extinction coefficients for the night of June 1. The observations of the local standards confirmed the values of the extinction coefficients determined from the primary standards. Transformation equations derived from the standard stars had the form:

$$v = V - 0.006\,(B-V) + 0.159\,(X - 1.25) + C_V \tag{1}$$

$$b = B + 0.105\,(B-V) + 0.243\,(X - 1.25) + C_B \tag{2}$$

where X is the airmass and C_V and C_B are the zero-point shifts for their respective filters. Comparing the transformed magnitudes of the standard stars with the values given by Graham and Landolt, we find rms residuals of 0.018 magnitudes in V and 0.006 magnitudes

in B.

The photometry of stars in the NGC 6388 field could be compared with photometry in three earlier studies, as shown in Table 1. First, we compared our photometry to the photoelectric photometry of a number of the standard stars in the field of NGC 6388 obtained by Alcaino (1981). Alcaino reported that photometry for 11 of the 26 stars used to calibrate his NGC 6388 data was found to be in good agreement with independent unpublished observations by K. C. Freeman. We were able to use 14 stars from Table I in Alcaino for comparison. The difference between our data set and that of Alcaino is somewhat large, which may result from only being able to compare our photometry to the fainter Alcaino standard stars.

A large number of comparisons could be made with the CCD photometry of Silbermann et al. (1994). We first matched the position of the stars in Table 3 of Silbermann et al. with our data. A number of discrepant values were found. With no image to compare from Silbermann et al. it is difficult to ascertain whether these stars were crowded or not. However, the majority of the magnitudes were in good agreement with our data.

A comparison to the HST B, V photometry obtained by Rich et al. (1997) of NGC 6388 was also made. Due to the compact nature of NGC 6388 it was difficult finding a large number of uncrowded stars on the images obtained at CTIO to compare with those found using the HST data, which looked only at the inner regions of the cluster. From a sample of 11 stars which were relatively uncrowded on our images we see that our ground-based photometry is brighter by about 0.025 mag.

3. Color-Magnitude Diagram

Figure 1a presents a CMD consisting of 19509 stars in the field centered on NGC 6388. Only stars with $\chi \leq 1.5$ are shown, where χ is a fitting parameter in Stetson's DAOphot programs. The red clump of the HB of the cluster can be seen at $V \sim 17.2$, $(B-V) \sim 1.15$. The main sequence of the field can be seen extending through the cluster's HB from $(B-V) \sim 1.0$ to ~ 0.7. Figure 1d shows the contribution of the field to the CMD of NGC 6388 in Figure 1a. Stars were chosen from a radius greater than 6.5 arcmin from the cluster center for Figure 1d (the tidal radius of NGC 6388 is 6.21 arcmin; Harris 1996).

The effects of differential reddening on the red giant branch (RGB) can be seen in the figures. This is especially notable in the luminosity function bump on the RGB at $V \sim 17.8$, $(B-V) \sim 1.3$. A closer analysis of this feature could shed light on the helium content of NGC 6388 (Sweigart 1978; Fusi Pecci et al. 1990; Zoccali et al. 1999; Bono et al. 2001; Raimondo et al. 2002).

Figure 1b shows all stars within 1.7 arcmin from the cluster center, giving the closest fit to the area of NGC 6388 observed by Rich et al. (1997). Because of crowding toward the center of NGC 6388, we could obtain good photometry for many fewer stars in the inner region than was possible with WFPC2. The number of HB stars detected in the WFPC2 images is about 1350 for NGC 6388 (Zoccali et al. 2000) and 1470 for NGC 6441 (Zoccali 2000, private communication). In contrast, we were able to obtain good photometry for only $\sim$ 70 HB stars within the central 1.7 arcmin radius circle of NGC 6388, a number considerably smaller than we were able to observe close to the center of NGC 6441 (Paper I). As a result, it is difficult to use Figure 1b to identify any HB slope in the V, $B-V$ CMD.

4. Variable Stars

4.1. Discovery of New Variable Stars

All variables were found with the same two methods as used for NGC 6441 (see §4.1 of Paper I). The time coverage of our observations is well suited for the discovery of short period variability, but not for the detection of long period variables. With the exception of stars falling outside of our field of view, all of the probable short period variable stars previously known were recovered during our variable star search. In addition, 28 probable new variable stars were detected. In crowded regions close to the cluster center, the B photometry proved superior to the V photometry for identifying variable stars, presumably because of the lesser interference from bright red giant stars. Finding information for the new variable stars is given in Table 2, where X, Y are the coordinates of the variables on the CCD [the cluster center is assumed to be at (1075.4,1064.4)] and $\Delta\alpha$, $\Delta\delta$ are the differences in right ascension and declination from the cluster center (in arcsec). Finding charts for the variables can be seen in Figure 2.

4.2. RR Lyrae stars

The variable stars have been studied previously by Hazen & Hesser (1986) and Silbermann et al. (1994). In the field of NGC 6388, the number of probable RRL has been increased from 10 to 14. Figure 3 shows the position of these stars within the CMD of NGC 6388. Of the previously known cluster RRL, only V24, which lies outside our field of view, was not rediscovered. The mean properties of the individual RRL, and the one δ Scuti or SX Phe star, found in this survey are listed in Table 3. The periods determined for the known RRL, using the phase dispersion minimization program in IRAF, are found to be in good agreement with those found by Hazen & Hesser and Silbermann et al. Spline fits

were used to determine the magnitude weighted and luminosity weighted mean magnitudes, $(B-V)_{\rm mag}$ and $\langle V \rangle$, respectively. Figure 4 shows the light curves for the individual variable stars, where the displayed light curves are those of the RRL, the Population II Cepheids (P2Cs), the eclipsing binaries, the δ Scuti or SX Phoenicis variable, and the variables with uncertain classification, in that order.

The accuracy of the periods found in our survey is $\pm$0.001d to $\pm$0.002d, depending on the scatter and completeness of the light curve. Tables 4 and 5 list the photometry for the individual variable stars.

Light curves were analyzed by Fourier decomposition using the equation,

$$mag = A_0 + \sum A_j \cos(j\omega t + \phi_j). \tag{3}$$

It has been shown (e.g., Clement & Shelton 1997) that RRab and RRc stars fall into distinct regions in a A_{21} vs. ϕ_{21} plot, where $A_{21} = A_2/A_1$ and $\phi_{21} = \phi_2 - 2\phi_1$. As found by Simon & Teays (1982), Figure 5 shows for those RRL with clean light curves that the RRab fall at values greater than A_{21} of 0.3 and the RRc fall below. Table 6 lists the values of the Fourier parameters, where $A_{j1} = A_j/A_1$ and $\phi_{j1} = \phi_j - j\phi_1$. The errors in the phase differences are based on Eq. 16d in Petersen (1986). We showed in Paper I that Fourier decomposition parameters can be used to determine if a star is a RRc variable or an eclipsing binary at twice the period. Although the method proved useful, there were no cases in NGC 6388 where this method was needed.

Shown in Figure 6 are the period-amplitude diagrams for NGC 6388 given in B and V. There is one RRab variable, V17, whose amplitude appears to be low for its period. This may be due to blending effects. However, this variable does not show the shift toward redder colors seen in certain RRab stars in NGC 6441 which were suspected of having

blended images (see Paper I). It should be noted that the Blazhko Effect can also reduce the amplitudes of RRab stars, but our observations do not extend over a long enough time interval to test for the presence of this effect. As with NGC 6441, we see that NGC 6388 lacks a significant gap between the shortest period RRab and the longest period RRc.

4.3. Notes on Individual Variable Stars

V17 - The amplitude appears to be low compared to the other fundamental mode RRL. There is some scatter in the curve indicating a possibility of blending. The ratio of the B to V amplitudes is not unusual, providing no indication that an unresolved blend with a different colored star has affected the photometry. Its mean magnitude is somewhat brighter than the other fundamental mode RRL.

V20 - There is scatter in the curve. It falls among the other cluster first overtone RRL in the CMD.

V26 & V34 - These two stars are similar in that they both are short period RRc stars and are unusually faint when compared to the other RRL. Their amplitudes are somewhat larger than the other short period RRc stars, as well. Both stars would have to be dereddened by an unusually large amount to move them back among the other RRc stars of NGC 6388. It may be that these two stars are actually nonmembers of the cluster.

V29 - P2C variable. Previously designated as a field RRL by Silbermann et al. (1994). No V data were available due to saturation. For this reason, the B data were placed on the standard system using a zero-point shift of +3.829.

V30 - This star fits in the CMD with the other fundamental mode RRL. The best fit to the data is a period around 0.939d. There is a gap in the data near maximum light through descending light. This, along with scatter in the curve, makes finding the best

period difficult.

V32 - (S1, Silberman et al.) A long period RRc type variable with some scatter in the curve.

V35 - One night of observations of this variable (night 4) falls at a different phase and amplitude as compared to the other nights, as shown in Figure 7. Taking that night out, the data fit the period of 0.299 d. See §5.2 for more discussion.

V18 and V36 - P2C variables. The light curves in V tend to have more scatter due to reaching the saturation limit of the CCD. Crowding in the cluster is also likely to contribute to the scatter found in the light curves since both stars are found near the center of the cluster.

V37 - A probable P2C variable. The maximum period fit to the data is 10 days due to the length of the observing run. The magnitude of the star gets fainter for the first four nights of observations, while the second four nights of observations show a clear maximum.

V44 - From the shape of the curve, location in the CMD, and the period, this star is either of δ Scuti or SX Phoenicis type. From the magnitude of the star, it is unlikely that it is a member of NGC 6388.

V48 - Shows definite variability, but has a lot of scatter in the light curve making classification difficult and the magnitude and color unreliable. The B light curve does look like that of a c-type RRL. The mean magnitude of the variable places it along the HB, although slightly bluer than the other RRc.

V49 - (S2, Silberman et al.) A lot of scatter in the light curve makes the exact classification uncertain, although the B curve looks somewhat like that of a c-type RRL. Its mean magnitude and color place it among the other probable cluster RRc.

V50 - The light curves show scatter, especially in B, making classification uncertain and the mean magnitude and color unreliable. The V curve looks to be RRc type.

V51 - This star shows definite variability, but a large amount of scatter exists. Its magnitude and color, although somewhat unreliable, place the variable among the other probable NGC 6388 RRL.

V52 - A variable that falls among the first overtone RRL in the CMD of NGC 6388. An unusual light curve shape, which shows a sharp decrease in magnitude after maximum, makes its classification uncertain. This variable is found next to a much brighter star, which may be affecting the photometry.

V53 - (S3, Silbermann et al.) This star shows definite variability, but we were only able to observe it when the star was increasing in brightness. Therefore, the magnitude, color, and period given for this variable are not reliable.

V55 - A likely c-type RRL. The variable falls among the other probable RRc of NGC 6388. A gap occurs during the rising light in the light curve up to near maximum light, making the exact classification uncertain.

V56 - Scatter in the data makes this star's classification uncertain. The mean magnitude of the variable places it along the HB of NGC 6388.

S4 (Silbermann et al.) - We were unable to find any variability, although crowding may be an issue.

4.4. Reddening

Reddenings for the RRab stars of NGC 6388 were determined using Blanco's (1992) method as outlined in Paper I. We calculated the reddenings for the RRab stars with good

$(B-V)$ light curves listed in Table 7 by using the averaged photometry in the phase range 0.5–0.8 and Eqs. 3 and 7 in Blanco.

The mean reddening value for the 4 RRab stars which are believed to be probable members of NGC 6388 is $E(B-V) = 0.40 \pm 0.03$. The range in reddening values agrees with previous determinations that NGC 6388 is subject to differential reddening, although the range is not as large as that of NGC 6441. The smaller range in differential reddening may be due to the smaller sample of RRab stars, but it is most likely due to NGC 6388 being further away from the Galactic plane.

Silbermann et al. (1994) determined, in a similar fashion, that the reddenings for V17 and V29 are 0.48 and 0.47, respectively, with uncertainties of ± 0.04. One reason for the discrepancies between the reddenings determined by this survey and that of Silbermann et al. is their use of $\Delta S = 8$, corresponding to a metallicity lower than the one adopted in this paper ($\Delta S = 3.22$). Another explanation for the differences in reddenings may be the high scatter in the light curves found by Silbermann et al. Alcaino (1981) derived the reddening of NGC 6388 to be $E(B-V) = 0.41$ from the color of the giant branch as compared to that in 47 Tuc. Zinn (1980) and Reed et al. (1988) obtained $E(B-V) = 0.35$ and 0.39, respectively, from their analysis of the integrated cluster light. The Schlegel, Finkbeiner, & Davis (1998) reddening value is 0.415 for NGC 6388.

We find the mean magnitude of the RRL, leaving out those RRL of uncertain classification, to be $\langle V_{RR} \rangle = 16.85 \pm 0.05$ and 16.93 ± 0.6 without and with the two faint RRc stars V26 and V34, respectively. If we assume $A_V = 3.2E(B-V) = 1.28$, and if M_V for the RRL is between +0.5 to +0.8, then the distance modulus for NGC 6388 is in the range of 14.77 to 15.07 mag for the case where we do not include V26 and V34. The resulting distance to the cluster would be from 9.0 to 10.3 kpc. For comparison, Harris (1996) lists a distance of 11.5 kpc to NGC 6388 with a reddening of $E(B-V) = 0.40$,

$V_{HB} = 17.25$, and $M_V(HB) = 0.71$. The fainter $\langle V_{RR} \rangle$ value would only increase the distance by approximately 0.3 kpc.

There is some question as to whether or not there is a metallicity spread among the stars in NGC 6388 (see §5.6). It is therefore interesting to see how the reddening derived from the RRab stars depends on the adopted metallicity. If the metal abundances of the RRL were much lower than that which we have adopted, they would have less line blanketing and the reddenings which we would derive would be greater. For example, if we had adopted [Fe/H] = −2.0, our derived reddening value for NGC 6388 would increase by 0.05 mag, giving a reddening significantly larger than found by most other methods.

It should be emphasized that the type of RRL in NGC 6388 may be different in nature from those which Blanco used in establishing his relationship between metallicity, period, and intrinsic color. As was done for NGC 6441, we have assumed that Blanco's (1992) formula applies to the RRab stars in NGC 6388. This may not be the case if, as is presented in this paper, the RRab stars in NGC 6388 are unusually bright for their metallicity, although the reddening derived in this study matches well with those from other studies.

4.5. Cepheids

Silbermann et al. (1994) found a bright variable, V29, which they believed to be a foreground RRL. We find this star together with V18 from Hazen & Hesser (1986), and two additional variables to be P2Cs. The mean properties of these variables are listed in Table 8. V18 was listed by Hazen & Hesser (1986) as a star with a period < 2 days. Of the 4 Cepheids found, 3 have periods of less than 10 days, making them members of the subset of P2Cs known as BL Herculis stars. As was noted in §4.3, V37 has a period of around 10 days, classifying it as a W Virginis-type P2C. Although V29 was saturated in V, using

light curve fitting programs created by Andrew Layden (Layden & Sarajedini 2000, and references therein) we were able to find $\langle B \rangle = 16.035$. From the zero-point shift (§4.3), V29 seems to be oddly brighter than V18 and V36. The reason for this difference is uncertain, although crowding may be an effect. The properties of the Cepheids are discussed further in §5.3.

1.6. Eclipsing Binaries and LPVs

We were able to find a number of eclipsing binary stars within our field of view, which are not likely to be members of NGC 6388. Only V14 listed by Hazen & Hesser (1986) was recovered. Table 9 lists photometric data for the binary stars. Due to our sampling it was somewhat difficult to determine accurate periods for detached binaries.

The time coverage of our observations was not suitable for the detection of long period variables (LPVs). Only two of the previously suspected variables in NGC 6388 were determined to be LPVs by this survey, V4 and V12. Three additional LPVs were found, V45, V46, and V47. The LPVs found by this study and their locations can be found in Table 2.

5. Discussion

5.1. General Properties of NGC 6388 RR Lyrae

We compare the average properties of the RRL in NGC 6388 and NGC 6441 to those of RRL in Oosterhoff types I and II clusters, M3 and M15, in Table 10. The RRab in NGC 6388 have unusually long periods for a metal-rich cluster, as was shown in Pritzl et al. (2000). From what is known of the periods of metal-rich field RRL, one would expect the

mean period of the RRab stars in NGC 6388 to be even shorter than those from Oosterhoff type I clusters. In fact, the mean period of the RRab in NGC 6388 is longer than in typical Oosterhoff type II clusters, as was also the case for NGC 6441. It is also interesting to note the unusually high N_c/N_{RR} ratio (where N_c is the number of RRc stars and N_{RR} is the total number of RRL in the system) for NGC 6388.

In Figure 8 of Paper I, we showed how the trend of decreasing period with increasing metallicity for the Oosterhoff types I and II globular clusters is broken by the mean periods of the RRab stars in NGC 6388 and NGC 6441. It appears, as was concluded by Pritzl et al. (2000), that NGC 6388 does not fall into either Oosterhoff group according to its metallicity. However, it has been suggested that the Oosterhoff dichotomy may be due to evolutionary effects. Lee, Demarque, & Zinn (1990) postulated that the RRL in Oosterhoff type II clusters have evolved away from a position on the zero-age HB (ZAHB) on the blue side of the instability strip. This leads to the RRL in Oosterhoff type II clusters having longer periods and higher luminosities than the RRL in Oosterhoff type I clusters, whose ZAHBs are thought to be more heavily populated in general. This idea has been used to argue that the location of RRab stars in the period-amplitude diagram may be more a function of Oosterhoff type than metallicity (Clement & Shelton 1999; Lee & Carney 1999; Clement & Rowe 2000). While most of the RRab in NGC 6441 fall along the Oosterhoff type II line as defined by Clement (2000; private communications; see Fig. 7 in Paper I), the RRab in NGC 6388 appears to be scattered in the period-amplitude diagram (see Figure 6). Two of the RRab fall at longer periods than given by the Oosterhoff type II line, while two others fall in-between or near the Oosterhoff type I line (see §5.7 for further discussion).

The derived properties of the RRc stars can also give some indication to the Oosterhoff type of the cluster (e.g., Table 4 of Clement & Rowe 2000). Using the Fourier parameters in Table 6 along with Eqs. 2-5 in Clement & Rowe, which derive from Simon & Clement

(1993a, 1993b), we calculated the masses, luminosities, temperatures, and absolute magnitudes listed in Table 11 for the RRc in NGC 6388. Only those RRc's with errors in the ϕ_{31} measurement less than 0.50 and periods less than 0.44d were included. The mean values for the mass, $\log(L/L_\odot)$, $T_{\rm eff}$, and M_V are 0.48 $M_\odot$, 1.62, 7495 K, and 0.82. As with the derived properties of the RRc variables in NGC 6441, the masses for the RRc stars in NGC 6388 are low (see Paper I for further discussion). Placing NGC 6388 in Table 4 of Clement & Rowe according to the mean $\log(L/L_\odot)$ and $T_{\rm eff}$ values, we see that NGC 6388 falls among the Oosterhoff type I clusters. This contradicts what was indicated by the location of the RRab stars in the period-amplitude diagram. These results further illustrate the difficulty in classifying NGC 6388, along with NGC 6441.

We also calculated the properties for the RRab stars using the Jurcsik-Kovács method (Jurcsik & Kovács 1996; Kovács & Jurcsik 1997). After correcting the Fourier parameters in Table 6 to work in the sine-based Jurcsik & Kovács equations, we derived the parameters shown in Table 12 using Eqs. 1, 2, 5, 11, 17, and 22 from Jurcsik (1998), correcting the values of $\log(L/L_\odot)$ and $\log T_{\rm eff}$ by +0.1 and +0.016 (Jurcsik & Kovács 1999). The mean values for the mass, $\log(L/L_\odot)$, $\log T_{\rm eff}$, M_V, and [Fe/H] are 0.56 $M_\odot$, 1.69, 3.82, 0.66, and -1.21, respectively. When compared to the data in Figure 1 of Jurcsik & Kovács (1999), the mean value of $\log(L/L_\odot)$ for the RRab in NGC 6388 is about 0.1 brighter than their data at a metallicity of [Fe/H] $= -0.60$ which agrees with the idea that the RRL in NGC 6388 are unusually bright for the metallicity of the cluster. Meanwhile, the mean $\log T_{\rm eff}$ values are about 0.02 lower and the mean mass is consistent with the data given in Jurcsik & Kovács (1999). The derived mean value for M_V, which does not include the $\log(L/L_\odot)$ correction of +0.1 from Jurcsik & Kovacs (1999), is about 0.49 mag brighter than given by Eq. 5 in Kovács & Jurcsik (1996) using [Fe/H] $= -0.60$.

Similar to what we found for the RRab in NGC 6441 (Paper 1), the metallicity

derived from the RRab in NGC 6388 is unusually low, [Fe/H] = −1.2 (−1.4 on the Zinn & West 1984 scale). It is uncertain how well the Jurcsik-Kovács method applies to RRab of unusually long periods. Moreover, it is hard to reconcile the RGB morphology of NGC 6388 with that of more metal-poor globular clusters (Raimondo et al. 2002). While a lower metallicity may explain the blue extension to the HB, it would not explain the red clump. We discuss the possibility of a metallicity spread in §5.6.

In Figure 8 we present an updated histogram for the period distribution of the RRL in NGC 6388 according to their period. As seen in Pritzl et al. (2000), this provides an additional way to demonstrate how the properties of the RRL contradict the metallicity of the parent cluster. The number of RRc in NGC 6388 is high even when compared to Oosterhoff type II clusters rather than being the relatively small number expected for the more metal-rich Oosterhoff type I clusters.

Another way in which NGC 6388 is distinguished from the typical Oosterhoff groups is the high ratio of long period ($P > 0.8$d) RRab. Although there is only a small number, 50% (2 of 4) of the RRab have longer periods. The large proportion of long period RRab, a property shared by NGC 6441 (Pritzl et al. 2000, 2001), is not seen in other globular clusters.

5.2. RRc Variables

The existence of RRL is unusual in globular clusters as metal-rich as NGC 6388. The presence of RRc is especially unusual due to the typically red HB morphology associated with metal-rich globular clusters. This provides a unique opportunity to investigate the properties of these stars in an environment not seen in other globular clusters. Although the RRc stars in NGC 6388 span a wide range of periods, the mean period is 0.36d which is

comparable to the value for a typical Oosterhoff type II cluster (see Table 10).

As was noted with NGC 6441, the RRc stars in NGC 6388 have some distinguishing features. One such feature is the bump in the light curve seen during the rise to maximum brightness. While this bump occurs at a phase of about 0.2 before maximum for the RRc with periods between 0.33 d and 0.37 d, the RRc with periods greater than 0.4 d have the bump occurring nearer phase 0.3 before maximum. No bumps are seen in the light curves for the RRc with periods less than 0.31d.

Layden et al. (1999) originally pointed out that the RRc stars in NGC 6441 may exhibit longer than usual rise times. Similar to NGC 6441 (Layden et al. 1999; Paper I), the range of rise times for the RRc stars in NGC 6388 is about 0.45 to 0.50 in phase with the longer period stars having longer rise times. Compared to the range listed in Layden et al. for RRc stars from the *General Catalog of Variable Stars* (Kholopov 1985), 0.32 to 0.46, the rise times seen in the RRc stars of NGC 6388 are somewhat longer than usual.

The RRL in NGC 6388 show an unusually short gap between the longest period RRc star and the shortest period RRab star, similar to NGC 6441 (Paper I). Van Albada & Baker (1973) found that a gap of about 0.12 should be expected between the logarithms of the periods of the shortest period RRab star and the longest period RRc star, assuming that the RRab and RRc stars have the same mass and luminosity, and that there exists a single transition line in effective temperature between the first overtone and fundamental mode pulsation domains in the HR diagram. Many globular clusters show such a gap, indicating that these assumptions may hold for most globular clusters. The absence of such a gap in NGC 6388 and NGC 6441 implies that one or more of the assumptions is incorrect in their case.

The RRc star V35 deserves a special mention. As noted in §4.3 and seen in Figure 7, the phase and amplitude of the star are different on the night of 29 May than on the other

nights. There are no nearby stars affecting the photometry and there is no indication that night has any problems since the photometry for other variables shows no anomalies. It may be the case that the star is going through a mode switch or mode instability. More photometry of V35 may help clear up this issue.

An interesting feature seen in NGC 6388, but not in NGC 6441, is the occurrence of "short" period c-type RRL. As seen in the period-amplitude diagram for NGC 6388 (Figure 6), the c-type RRL, with the exception of V35, seem to fall into three distinct groups: The "longer" period RRc centered at $\log P = -0.288$, the "intermediate" period RRc centered at $\log P = -0.459$, and the "shorter" period RRc centered at $\log P = -0.617$. There does not appear to be any distinction between the shorter period RRc found in NGC 6388 and the more "intermediate" period RRc, according to their Fourier parameters, but there is a clear distinction when the Fourier parameters of the longer period RRc are compared to those of the "intermediate" period RRc (see §5.5). The light curves of the shorter period RRc seem to show more scatter during maximum light as compared to the light curves of the other RRc members of NGC 6388, and are slightly more asymmetric, although the photometry obtained in this survey is not accurate enough to make a conclusive argument for this. It is of interest to note that two of the three shorter period RRc stars are fainter than the other probable RRc of NGC 6388, as shown in Figure 3 and discussed in §4.3. It cannot be determined if this effect is due to the differential reddening in NGC 6388, but it can be said that these two RRc stars, which also happen to be the shortest period RRc, do not fall in the same part of the NGC 6388 field.

It has been argued by some authors that short period RRc stars with $P < 0.35$d and amplitudes less than 0.3 mag may in fact be pulsating in the second overtone mode (e.g., Clement, Dickens, & Bingham 1979; Walker 1994; Walker & Nemec 1996). The MACHO collaboration found a maximum in the Large Magellanic Cloud RRL period distribution

at 0.28 days (Alcock et al. 1996), arguing that this corresponded to the second overtone, RRe, stars. Alcock et al. found that the RRL located about this range showed skewed light curves, as was modeled by Stellingwerf et al. (1987). Clement & Rowe (2000), using the RRc stars in ω Centauri (NGC 5139), argue that a number of the shorter period stars were pulsating in the second overtone mode. They showed that these RRc stars also have low amplitudes ($A_V < 0.3$ mag). Overall, the short period RRc stars in NGC 6388 do not have amplitudes as low as these stars. However, if we disregard V26 and V34, which may be nonmembers (§4.3), the remaining two RRc stars, V16 and V35, do have low amplitude, making them similar in both period and amplitude to the stars in ω Cen which Clement & Rowe identified as second overtone pulsators. However, a case has also been made that short period RRL of this type are not second overtone pulsators. Kovács (1998) argued that these variables are RRc variables at the short period end of the instability strip. It is beyond the scope of this paper to argue for or against the classification of the shorter period RRc-type stars as second overtone pulsators. In any case, further observations of these variables would help to improve pulsation models and help explain why such a large range in RRc periods exists (0.24 - 0.56 days) in NGC 6388.

5.3. Cepheids

The occurrence of P2Cs in globular clusters is not uncommon. Yet, if the probable Cepheids found in the field of NGC 6388 are indeed members of this cluster, NGC 6388 would be the most metal rich globular cluster known to contain Cepheids. A review by Harris (1985) listed the globular clusters containing Cepheid (16 GCs) or RV Tauri variables (5 GCs). Harris confirmed that the globular clusters which contained P2Cs also have blue horizontal branches (Wallerstein 1970). It was further noted by Harris that BL Her, P2Cs with periods < 10 days, may be most frequent in clusters which have extended blue tails on

the horizontal branch. Smith & Wehlau (1985) found that all of the globular clusters known to contain Cepheids have $B/(B+R) > 0.50$, where B is the number of stars blueward of the RRL gap and R is the number of stars redward of the RRL gap. The reverse is not true, however. All clusters with $B/(B+R) > 0.50$ do not contain Cepheids. Smith & Wehlau also noted that W Vir stars, P2Cs with periods > 10 days, tend to be in the most metal-rich of the globular clusters which have blue HBs. Finally, it was also shown that the clusters with Cepheids are also the brighter, more massive, clusters, especially those clusters which have two or more Cepheids. In a summary of the variable stars in Galactic globular clusters, Clement et al. (2001) use the HB ratio $(B-R)/(B+V+R)$, where B and R follow the above definitions and V is the number of RRL, finding that most globular clusters with P2Cs have $(B-R)/(B+V+R) > 0$, with two exceptions: NGC 2808 and Palomar 3. Pal 3 provides the most serious challenge to explain since it lacks any blue extension to the HB (Borissova, Ivanov, & Catelan 2000).

NGC 6388 does exhibit some of the features listed above. It does have a blue component to its HB. Although the $B/(B+R)$ fraction was not determined for NGC 6388 in this study due to the high contamination from field stars, according to the number counts in Zoccali et al. (2000) $B/(B+R) = 0.15$. Even though this disagrees with the idea that P2Cs are only found in globular cluster with $B/(B+R) > 0.50$, the relatively large number of BL Her stars found in NGC 6388 agrees with Harris' (1985) idea that they are more frequent in clusters with extended blue tails. The one candidate W Vir star in NGC 6388 follows the idea that these stars tend to be in the most metal-rich of the globular clusters with well-developed blue HBs. NGC 6388 is also one of the brightest globular clusters known in the Galaxy, confirming the tendency of clusters containing Cepheids to be brighter than those that do not.

There has been some debate on the P2C period-luminosity relations and on the

question of whether or not P2Cs pulsate in both the fundamental and first overtone modes or solely in the fundamental mode (see Nemec, Nemec, & Lutz 1994; McNamara 1995; and references therein). For this study, we would like to have an idea of the absolute magnitudes of the Cepheids in NGC 6388 in order to estimate the distance to the cluster and the absolute magnitude of the RRL. Using Eqs. 7, 8, 11, and 12 from McNamara (1995), we calculated the absolute magnitudes listed in Table 13. It should be noted that the absolute magnitudes calculated for the P2Cs in Nemec, Nemec & Lutz, which were also used by McNamara, are based on the distance moduli and reddenings of the systems for which they are associated. Although there is some differential reddening across the face of NGC 6388, we use the mean reddening of the cluster, $E(B-V) = 0.40$, in determining the extinctions, $A_V = 3.2E(B-V) = 1.28$ and $A_B = 4.1E(B-V) = 1.64$, to deredden the Cepheid magnitudes. We want to restate that the mean magnitudes of these stars are somewhat uncertain due to the scatter and gaps in the light curves (see Figure 4). Examining the resulting distances in Table 13, V29 and V37 have distances much less than V18 and V36. We noted previously (§4.5) that V29 seemed unusually bright for its period. The precise $\langle B \rangle$ magnitude is uncertain since the star is saturated in V. For V37, the exact period is uncertain due to an incomplete light curve, and thus its magnitude may also be uncertain. The scatter in the light curve also makes the magnitude uncertain. It also could be that V29 and V37 are not members of NGC 6388, but this seems unlikely due to their proximity to the cluster center (see Figure 2). The distance we find using the visual estimates of V18 and V36 is 10.6 kpc, which matches well with the distance estimates made from the RRL.

If we adopt the distance of 10.6 kpc and $A_V = 1.28$, we find $M_{V,\mathrm{RR}} = +0.44$ for $V_{\mathrm{RR}} = 16.85$ mag. This value is higher than one would expect for the metallicity of NGC 6388. For example, given [Fe/H] = −0.60 and using Eq. 7 in Lee, Demarque, & Zinn (1990), $M_{V,\mathrm{RR}} = +0.72$ on their scale.

An interesting question to ask is: Why does NGC 6388 contain Cepheid stars, but NGC 6441 does not? It is possible that our survey was incomplete in finding any Cepheids in NGC 6441 (Paper I), but this does not seem to be the case since no Cepheids were found in the survey of Layden et al. (1999), either. Assuming that our survey was complete, and no Cepheids occur in NGC 6441, the answer to this question may give hints as to the origin of the Cepheids. Both clusters are among the brightest known and both have similar HB morphologies. Along with having similar metallicities, it would seem that if one of this pair of clusters contained Cepheids, the other would have them too. It was suggested by Smith & Wehlau (1985), from the models of Mengel (1973) and Gingold (1976), that P2Cs may evolve from horizontal branch stars which already have low envelope masses. Sweigart & Gross (1976) predicted that clusters with blue horizontal branches *and* higher metal abundances would produce horizontal branch stars with especially low envelope masses. It can be seen in the CMDs for NGC 6388 and NGC 6441, by Rich et al. (1997), that the blue "tail" in NGC 6388 appears to be more populated than in NGC 6441. This may explain the difference between NGC 6388 and NGC 6441, although it may just be a selection effect since we are talking about such small numbers.

5.4. Period-Amplitude Diagram

We revisit the period-amplitude diagram in Figure 9 and compare the RRab in NGC 6388 to the RRab in other globular clusters (M15: Silbermann & Smith 1995, Bingham et al. 1984; M68: Walker 1994; M3: Carretta et al. 1998; 47 Tuc: Carney, Storm, & Williams 1993) and metal-rich field RRab. As discussed in Pritzl et al. (2000), the RRab in NGC 6388 fall at unusually long periods compared to field RRab of similar metallicities. Similar to NGC 6441 (Paper I), NGC 6388 breaks the trend of increasing period with decreasing metallicity for a given amplitude. Although no direct measurements of the

metallicity for the RRL in NGC 6388 are available (see §5.6), it is interesting to see that V9 of 47 Tuc ([Fe/H] = −0.76) falls in the same general location as the RRab in NGC 6388 and NGC 6441, though shifted away from the mean locus occupied by the RRL in these two globulars by $\Delta \log P \approx +0.1$ at fixed amplitude.

The RRab in NGC 6388 even fall at longer periods when compared to the RRab in the Oosterhoff type II cluster M15. This seems to contradict our previous finding that the RRab in NGC 6388 are scattered about a singular locus for all Oosterhoff type II globular clusters as given by Clement (2000, private communication) (see §5.1). An important tool in creating these lines was the compatibility condition (Jurcsik & Kovács 1996) which helped in determining which light curves are "normal" or not. An analysis done in Paper I (cf. §5.3) of the sample of RRab in M15 showed that a few of these stars which satisfy the compatibility condition fall between the Oosterhoff lines given by Clement. It is interesting to note that only V22 of NGC 6388 is close to complying with the compatibility condition (column 9 of Table 6). Although our time-coverage is not long enough to observe the Blazhko Effect, it would seem unlikely that all of the RRab in NGC 6388 would show this effect given that only about 20% of the RRab stars are thought to show the Blazhko Effect among the field and globular cluster populations alike. Also, the number fraction possibly decreases with increasing metallicity (see Table 5.3 in Smith 1995 and references therein).

Another way to examine how the RRab in NGC 6388 compare to those in M15 is to analyze the period shift of NGC 6388 from M3. Due to the small number of RRab stars in NGC 6388, it is difficult to make a general statement on the period shift. Two of the RRab, V17 and V22, appear to have period shifts close to those for the RRab in NGC 6441 (~ 0.08 in $\log P$; see §5.3 in Paper I), but the other two, V21 and V28, have period shifts more on the order of 0.15 implying they are somewhat brighter than the other RRab in NGC 6388 and NGC 6441. As can be seen from Figure 9, this property is shared by V9 in

47 Tuc. However, our photometry does not indicate that V21 and V28 are unusually bright compared to the other RRab.

5.5. Comparisons to Long Period RR Lyrae in ω Centauri

It has been shown that ω Cen is a globular cluster containing mostly RRL similar to those in Oosterhoff type II clusters along with a smaller population similar to RRL in Oosterhoff type I clusters (Butler et al. 1978; Caputo 1981; Clement & Rowe 2000). It is interesting to note that ω Cen also contains a number of longer period RRL similar to what is seen in NGC 6388 and which are not typically found in either Oosterhoff type I or Oosterhoff type II clusters. These longer period ($P > 0.8\ d$) stars are similar in both period and amplitude to the long period RRab in NGC 6388 and NGC 6441, although long period RRab form a much smaller fraction of the total RRab population in ω Cen than in those two clusters.

In addition to the longer period RRab stars, ω Cen contains a number of longer period RRc, similar to V20, V32, and V33 in NGC 6388. In Paper I we showed how the longer period RRc formed a distinct group at shorter ϕ_{21} in a ϕ_{21} vs. A_{21} plot for ω Cen (see §5.4, and Figure 11 in Paper I). This trend was also seen in NGC 6441. An examination of the ϕ_{21} and A_{21} values for the longer period RRc in NGC 6388 (Table 6) shows that the three RRc which stand apart from the rest of the RRc at shorter ϕ_{21} values in Figure 5 are indeed the three longer period stars.

In Figure 10, we plot a sample of ω Cen RRc stars according to their metallicity. The periods were taken from Kaluzny et al. (1997). When there was more than one entry for a single star, the values were averaged. The [Fe/H] values come from Rey et al. (2000). The RRc classifications were taken from Butler et al. (1978). There appears to be a slight

trend of increasing metallicity with decreasing period and increasing amplitude. The RRc of NGC 6388 in the period range of 0.3d to 0.4d fall among the more metal-rich RRc of ω Cen, while the longer period ones ($P > 0.45$d) fall among the RRc in ω Cen which have a more "intermediate" metallicity. Two other longer period RRc are included in this plot, V70 in M3 (Kaluzny et al. 1998; Carretta et al. 1998) and V76 in M5 (Kaluzny et al. 2000). Although the period of V76 is somewhat shorter than the periods of the other long period stars, it is unusually long when compared to the other RRc stars in M5. We emphasize that such long period RRc variables are extremely rare in either Oosterhoff type I or Oosterhoff type II globular clusters, no additional examples being known to exist besides V70 in M3 and V76 in M5.

The unusual nature of NGC 6388 and NGC 6441 is shown again by the occurrence of these longer period RRc stars. More importantly, as was discussed above, it may be that these stars hint at a more metal-poor component in NGC 6388 (and NGC 6441), with properties similar to the corresponding ones that give rise to the ω Cen long-period RRc's. In this paper we have assumed that the RRL in NGC 6388 have the same metallicity as the overall cluster value since no direct metallicity measurements for the RRL currently exist.

5.6. A Metallicity Spread in NGC 6388?

The possibility of a spread in metallicity in NGC 6388 and NGC 6441 was first proposed by Piotto et al. (1997). More recently Sweigart (2002) explored the metallicity-spread scenario through stellar evolution calculations. The models showed that the upward slope in the HB seen in NGC 6388 and NGC 6441 can be produced by a spread in metallicity assuming that all of the stars are coeval and that the mass loss efficiency, as measured by the Reimers (1975) mass loss parameter, is independent of [Fe/H]. (Please see Paper I for an in-depth discussion on the metallicity spread issue in this cluster and NGC 6441.)

In an attempt to produce synthetic CMDs for ω Cen, Ree et al (2002) also attempted to model the CMDs of NGC 6388 and NGC 6441. Their population models showed that two distinct populations could be contained within the broad RGBs of the two clusters. In addition, the HB could be explained by adding an older, metal-poor HB and a younger, metal-rich HB, with the age and metallicity spread being about 1.2 Gyr and 0.15 dex, respectively. Ree et al. went on further to suggest that if there is indeed a metallicity spread in NGC 6388 and NGC 6441, these two clusters may in fact be relicts of disrupted dwarf galaxies as has been suggested for ω Cen and M54. The one conundrum with this hypothesis is that, unlike ω Cen, where you have a mostly metal-poor population with some metallicity spread towards higher metallicities, for NGC 6388 and NGC 6441 one would have a mostly metal-rich population with a small metal-poor population. Their synthetic CMDs also failed to reproduce the sloping nature of the HB. In order to have self-enrichment up to such a high metallicity, a progenitor galaxy with which NGC 6388 and NGC 6441 may have been associated would have to have been much more massive than the Sagittarius dwarf spheroidal, or than the conjectured dwarf spheroidal progenitor of ω Cen.

Recently, Raimondo et al. (2002) argued that all metal-rich globular clusters should have tilted red HBs. In discussing the specific cases of NGC 6388 and NGC 6441, they felt that the slopes in the red HBs were real and not artifacts of differential reddening. Raimondo et al. also used the point where the HB magnitudes increase to make the blue tail as defined in Brocato et al. (1998) to match up more metal-poor globular clusters with well defined blue tails to NGC 6388. Matching the CMDs in this way allowed them to argue that the blue component of the HB of NGC 6388 cannot derive from metal-poor progenitors since there is not a corresponding large number of RGB stars blueward of the given RGB of the cluster. This provides an important constraint and challenge to the possibility of the blue HB in NGC 6388 and NGC 6441 being metal-poor. However, it should be noted that if NGC 6388 and NGC 6441 have metallicity spreads rather than two distinct populations,

the metal-poor RGB stars would scatter over a larger area blueward of the metal-rich RGB. This would serve to make the metal-poor giant stars less conspicuous than in the case where you have two distinct metallicities. In any case, more studies into this hypothesis should be done and clearly, metallicity determinations need to be made of the RRL in NGC 6388 and NGC 6441 to resolve this issue. It should be noted that Raimondo et al. did not address the presence of long-period RRL in NGC 6388 and NGC 6441, and did not provide a physical explanation for the presence of blue HB stars in these clusters.

5.7. Are NGC 6388 and NGC 6441 Oosterhoff Type II Globular Clusters? Evolutionary Constraints

Our preceding discussion has indicated that there are problems with the unambiguous classification of NGC 6388 and NGC 6441 into either Oosterhoff group (see also Pritzl et al. 2000, 2001). In a recent analysis of this problem, Clement et al. (2001) suggested that the period-amplitude relation of the RRab variables in NGC 6441 is most consistent with that cluster being classified as an Oosterhoff type II system (see also Walker 2000). As we have seen, the RRab variables in NGC 6388 scatter about the Oosterhoff type II region with some falling near the Oosterhoff type I regions of the period-amplitude diagram. Several authors (Lee et al. 1990; Clement & Shelton 1999; Clement et al. 2001) have proposed that evolution from ZAHB positions blueward of the instability strip may play an important role in determining the pulsational properties of RRL in Oosterhoff type II clusters. We thus need to consider whether the RRL in NGC 6388 and NGC 6441 could have evolved in this fashion from blue HB progenitors. To do this, we must address possible problems with the general evolutionary scenario in which RRL in Oosterhoff type II globular clusters are all evolving to the red from ZAHB positions on the blue HB.

This evolutionary scenario for Oosterhoff type II RRL raises the following key questions:

(1) Do blue HB stars spend enough time within the instability strip as they evolve redward to the asymptotic giant branch to produce the observed numbers of RRL in Oosterhoff type II globular clusters? (2) Does the predicted period-effective temperature relation for a given cluster depend on the stellar distribution along the blue HB? (3) Is the predicted period-effective temperature relation independent of metallicity?

Renzini & Fusi Pecci (1988) and Rood & Crocker (1989) have argued that blue HB stars do not spend sufficient time in the instability strip to account for the observed number of RRL in the Oosterhoff type II clusters. We decided to reanalyze these results by investigating the predicted loci and evolutionary timescales of blue HB models as they evolve across the instability strip in both the Hertzsprung-Russell (HR) and period-temperature diagrams. Given the range in metallicities among Oosterhoff type II clusters, and also the possibility of a metallicity spread in NGC 6388 and NGC 6441, we considered four metallicity values, namely: $Z = 0.0005$, 0.001, 0.002 and 0.006. A helium abundance $Y_{\rm MS} = 0.23$ was assumed in all cases. The new HB sequences computed for this analysis are based on the same assumptions as the models of Sweigart & Catelan (1998). In addition, we assumed an instability strip width $\Delta \log T_{\rm eff} \sim 0.085$ (Smith 1995), and the fundamental pulsation equation from van Albada & Baker (1971).

At any given metallicity, there is a critical mass $M_{\rm HB,ev}$ above which stars will evolve to the blue while crossing the instability strip, but below which stars will cross the instability strip only during their final redward evolution back to the asymptotic giant branch. Therefore, $M_{\rm HB,ev}$ defines the reddest possible HB morphology that a globular cluster could have and still produce exclusively redward-evolving RRL. In practice, one should expect the actual HB morphology of any globular cluster in which all RRL are indeed evolving to the red to be much bluer than defined by $M_{\rm HB,ev}$, due to the presence of lower-mass stars—in other words, "real clusters" do not have delta functions for their HB mass distributions.

They presumably cannot have higher HB masses than $M_{\rm HB,ev}$ or else they would not be Oosterhoff type II in the evolutionary sense described above. Table 14 gives the variation of $M_{\rm HB,ev}$ with Z, as well as some key number fractions in the resulting HR diagrams.

Figure 11 shows the actual HB tracks for specific ZAHB locations, where the tracks for $M_{\rm HB,ev}$ are labeled "a". Tracks "b" and "c" start their evolution at a bluer position on the ZAHB, corresponding to $(B-V)_0 = 0$ and -0.1; these are estimated to represent the peak of the blue HB distributions in NGC 6441 and NGC 6388, respectively—cf. Fig. 7 in Piotto et al. (1999). To illustrate the rate of evolution, each HB track is plotted as a sequence of points separated by a time interval of 200,000 yr. The thin vertical lines along each track denote the blue and red edges of the instability strip. It is obvious from Figure 11 that the bluest HB stars evolve rapidly through the instability strip when compared to those for $M_{\rm HB,ev}$. This is even more clearly illustrated in Figure 12 where we plot the ratio of the time spent in the instability strip to the time blueward of the instability strip for all sequences with $M \leq M_{\rm HB,ev}$ against the time-averaged value of $\log T_{\rm eff}$ over the part of the HB track blueward of the instability strip. This choice for abscissa gives a better indication of where the stars are coming from on the blue HB than the ZAHB value of $\log T_{\rm eff}$. Figure 12 shows how the fraction of the HB phase which a blue HB star spends in the instability strip decreases rapidly as $\log T_{\rm eff}$ increases. Overall the variation of V/B with $\log T_{\rm eff}$ is quite similar for all four metallicity values, although the maximum value of V/B does depend somewhat on the metallicity. We conclude that, on the basis of their evolutionary rates, only stars within a relatively small range in $\log T_{\rm eff}$ just blueward of the instability strip have a significant chance of producing redward-evolving RRL, irrespective of the cluster metallicity. In terms of Figure 11, this corresponds primarily to the region in-between "a" and "b," corresponding mostly to the color range $0 \lesssim (B-V)_0 \lesssim 0.2$.

The direct answer to the first question we posed at the beginning of this section is

that only a relatively small portion of those HB stars blueward of the instability strip would spend enough time in the instability strip to be detected as RRL. Therefore, in order to produce a rich Oosterhoff type II RRL population, one would need to have a very strong population of HB stars just blueward of the instability strip. This agrees with the conclusions of Renzini & Fusi Pecci (1988) and Rood & Crocker (1989), who point out that the redward evolving blue HB scenario might work for globular clusters which have relatively few RRL such as M92, but not for Oosterhoff type II clusters with more substantially populated RRL instability strips, such as M15. Based on our ground-based data, we find that NGC 6388 has a V/B ratio of approximately 0.20 to 0.33 depending on whether or not we include those RRL of uncertain classification. The highest ratio that can be derived from the HB simulations discussed below is approximately 0.08 to 0.085. Therefore, it appears that not all of the RRL in NGC 6388 could have derived from redward evolving blue HB stars.

In Figure 13 we have plotted the log P-log $T_{\rm eff}$ version of Figure 11. The dots are again separated by 200,000 yr, and the pulsation periods were calculated from van Albada & Baker (1971). This figure illustrates how the stars evolving from the blue HB occupy different loci in the log P-log $T_{\rm eff}$ diagram. It is important to bear in mind, in determining the period-temperature distribution for a given cluster, the strong dependence of the V/B ratio on the HB $T_{\rm eff}$. For example, there would have to be about 4 times as many "b" stars as "a" stars to produce the same number of RRL. For the "c" stars, the ratio is about 50-100 times. We also found that the locus of the corresponding tracks changes very little with metallicity for $Z = 0.0005$, 0.001, and 0.002. For these metallicities the decrease in mass with increasing Z compensates for the decrease in luminosity so that there is little change in the period. Thus, for Oosterhoff type II metallicities, the log P-log $T_{\rm eff}$ relation seems more a function of where the tracks come from on the blue ZAHB rather than their metallicity. On the other hand, there is a significant difference between $Z = 0.002$ and 0.006. The

smaller masses of the $Z = 0.006$ sequences cannot compensate for their lower luminosities. This result should be kept in mind when interpreting the Oosterhoff classification of bright, metal-rich RRL, such as V9 in 47 Tuc ([Fe/H] $\simeq -0.7$, [α/Fe] $\simeq +0.2$; Carney 1996), V1 in Terzan 5 (metallicity around solar; Edmonds et al. 2001), the field star AN Ser ([Fe/H] $\simeq -0.04$; Sweigart & Catelan 1998 and references therein)—and, of course, the RRL in NGC 6388 and NGC 6441.

Figure 14 shows a set of synthetic HB simulations for the $Z = 0.0005$ case, which is a metallicity representative of typical Oosterhoff type II globular clusters, particularly when α-enhancement is taken into account. These simulations were computed using SINTDELPHI, described in Catelan, Ferraro, & Rood (2001b). In all cases, we have assumed a mass dispersion $\sigma_M = 0.03\,M_\odot$, but truncated the (Gaussian) mass deviate at $M_{\rm HB,ev}$ in order to ensure that any RRL present is evolving to the red. In order to minimize the statistical fluctuations and better illustrate the main trends, 1500 HB stars were used in each simulation. The upper left panel of Figure 14 shows the case in which the peak of the HB mass distribution is very close to "a," corresponding to an input value $\langle M_{\rm HB}\rangle = 0.66\,M_\odot$. The subsequent panels show the variation in HB morphology and in the expected RRL properties as one decreases $\langle M_{\rm HB}\rangle$ in steps of $0.015\,M_\odot$. Figure 15 is the same as Figure 14, the only difference being that the CMD was zoomed on the region around the instability strip, in order to better illustrate the expected RRL luminosity distributions. Similarly, Figure 16 shows the corresponding location of the RRL in the $\log P - \log T_{\rm eff}$ plane. In the latter, both RRab and RRc variables are shown, the periods for the latter having been "fundamentalized." The lower envelope to the distribution of variables in the upper left panel is overplotted on all panels; this line corresponds closely to line "a" in the upper left panel of Figure 13. The mean shift in periods at fixed $T_{\rm eff}$ away from this line, as well as the corresponding standard deviation, is also indicated in the plots.

Figures 15 and 16 show that, with a distribution in $M_{\rm HB}$ peaked around "a," a natural concentration of the RRL towards the locus occupied by "a" occurs. However, even for this higher value of $\langle M_{\rm HB} \rangle$, the implied scatter in log P at fixed $T_{\rm eff}$ is not negligible, and may easily reach $\Delta \log P \approx 0.05$. Moreover, there is a tendency for the mean locus to shift towards longer periods with decreasing $\langle M_{\rm HB} \rangle$, implying that, apart from statistical fluctuations, globular clusters are expected to produce a longer period shift at fixed $T_{\rm eff}$ as the HB morphology gets bluer (see also Lee 1990). Note also that the scatter in log P at a fixed $T_{\rm eff}$ also shows a tendency to increase as the HB gets bluer. Such intrinsic scatter often corresponds to a significant fraction of the separation between Clement & Shelton's (1999) Oosterhoff type I and type II lines ($\Delta \log P \sim 0.1$). The dispersion of the RRL in the log P – log $T_{\rm eff}$ plane questions the definition of a single line where the Oosterhoff type II RRL should fall, even in the context of the redward evolving blue HB scenario; the scatter would naturally be even larger, had the models not been artificially truncated at $M_{\rm HB,ev}$. In this sense, it is worth noting that, in Fig. 2 of Clement & Shelton (1999), RRL's deviate from the Oosterhoff type II line at fixed amplitude by ~ 0.02, ~ 0.035, and ~ 0.02 in log P for M9, M68, and M92, respectively. Scatter away from the Oosterhoff type II line is also apparent in Fig. 10 of Clement & Rowe (2000).

It is important to note that the predicted period shift between the ZAHB and "a" is only a relatively small fraction of the actual period shift between Clement & Shelton's (1999) lines for the two Oosterhoff groups. It is only when the mean Oosterhoff type II distribution clusters around "b," not "a," that we obtain a period shift of approximately the correct size. A smaller (observed) period shift would be possible if, as predicted by synthetic HB simulations, stars in Oosterhoff type I globulars encompassed a relatively wide range in absolute magnitudes and periods at fixed color and temperature, respectively (see, e.g., Fig. 1a in Lee et al. 1990, and Figs. 2-3 in Catelan 1993). This, in turn, would be consistent with the results of Sandage (1990), who finds intrinsic scatter in the CMD

and in the log P – log $T_{\rm eff}$ diagrams of both Oosterhoff type II and type I globulars, such scatter being systematically more pronounced for the latter. In particular, in the case of a cluster like M3, with a continuously populated ZAHB across the instability strip from the red HB to the blue HB "tail" (see, e.g., Fig. 1 in Moehler 2001), a sharp dichotomy between "ZAHB" and "evolved" stars is certainly not predicted by the models. These results indicate that intrinsic scatter must be adequately taken into account when attempting to classify individual RRL in terms of Oosterhoff type (Clement & Shelton 1999; Clement & Rowe 2000).

We can now adequately address the second and third questions we proposed at the beginning of this section. As we have discussed above, in order to produce a significant number of RRL according to the redward evolving blue HB scenario, a globular cluster would need to have a very strongly populated blue HB just to the blue of the instability strip. Therefore, most of the RRL would fall along the same locus in the log P – log $T_{\rm eff}$ diagram, regardless of metallicity. However, it is possible to produce discrepant points in the log P – log $T_{\rm eff}$ diagram from those RRL which originate from HB stars bluer than those found close to the instability strip. The tradeoff is that one would not find as many of these stars due to their rapid evolution through the instability strip, unless of course the ZAHB mass distribution compensates for the variation in evolutionary timescales as a function of $M_{\rm HB}$.

Regarding NGC 6388 and NGC 6441, Table 14 clearly implies that, if these clusters are Oosterhoff type II in the evolutionary sense discussed above—that is, with their RRL evolving to the red—and if the RRL have the cluster metallicity $Z \approx 0.006$, then the HB morphology of the population to which these stars are associated must necessarily be characterized by:

$$(B-R)/(B+V+R) \gg 0.74$$
$$B/(B+V+R) \gg 0.76. \quad (4)$$

Increasing the helium abundance with increasing Z would lead to even more stringent requirements on the number ratios.

Obviously, the HB morphology of either NGC 6388 or NGC 6441 is not at all this blue. On the contrary, both these clusters have predominantly red HBs. Therefore, in order for NGC 6388 and NGC 6441 to be Oosterhoff type II clusters with all their RRL evolved away from the blue ZAHB, we must resort to some different explanation. We have the following alternatives:

i) Assume that all cluster stars have the same metallicity. Then the distribution in some quantity along the ZAHB—such as the total mass, helium core mass, helium abundance—must be intrinsically bimodal, the red HB component being decoupled from the RRL plus blue HB component. Even though in this case the constraints on the number ratio between blue and red HB stars are lifted, those on the number ratio between blue HB and RRL stars remain very tight, with $V/B \ll 0.3$ (cf. Table 14). These restrictions are even more severe if the cluster variables have a somewhat lower metallicity than $Z = 0.006$ (cf. §5.1), as can be seen from Table 14;

ii) We can also relax the requirement that all cluster stars have the same metallicity. This means that we can invoke a lower metallicity for the RRL plus blue HB component. Note, however, that, unlike in the "metallicity range" scenario of Sweigart (2002), the ZAHB *must* necessarily be depopulated in the RRL region, or the result will not be an Oosterhoff type II cluster with all RRL evolved from the blue. Therefore, a metal-poor component giving rise to RRL must necessarily be detached from the red HB component,

with no ZAHB stars populating the region between the blue HB and the red HB. In other words, if the range in temperatures on the NGC 6441 and NGC 6388 HBs is due to a range in metallicity, and if the clusters are Oosterhoff type II (with all variables evolved), it thus follows that their metallicity distributions must be bimodal. Note that this would be an even more dramatic bimodality than is thought to exist in ω Cen (e.g., Pancino et al. 2000). Such a bimodality, if indeed present, would help reconcile the predicted presence of short-period (near-ZAHB) RRL in Sweigart's (2002) scenario with the lack of such short-period RRL in NGC 6388 and NGC 6441.

It should be noted, in addition, that in either scenario the (sloped) red HB component must necessarily *not* produce RRL in any significant numbers, or else the "evolutionary Oosterhoff type II hypothesis" would break down; this, in turn, also limits the extent to which some of the physical parameters, such as the helium abundance, can vary along the red HB component (as thought to be necessary to produce the sloped HB that characterizes both NGC 6388 and NGC 6441; Sweigart & Catelan 1998). This is because HB stellar evolution naturally predicts that stars commencing their HB evolution just redward of the red edge of the instability strip will eventually evolve along "blue loops" and cross the instability strip, thus becoming blueward-evolving RRL. In particular, red HB stars with a fairly high helium abundance, which evolve along very extended blue loops during a significant fraction of their HB lifetime (compare, for instance, the $Y = 0.23$ HB tracks in Fig. 1 of Sweigart 1999 with the $Y = 0.43$ HB tracks presented in the same figure, as well as with the helium mixing tracks in Fig. 3 of that paper), would lead to a population of RRL clearly violating the assumption that RRL in Oosterhoff type II globular clusters are all evolving to the red.

Given the evolutionary issues discussed above, it is conceivable that the particular selection criteria used in Clement & Shelton (1999) in defining their "normal" stars is too

strict in the sense of leading to the rejection of many of those stars which are naturally expected to scatter around their Oosterhoff types I and II lines. If so, this might alleviate the requirement that RRL in Oosterhoff type II clusters be evolved away from the blue ZAHB—and, conversely, that RRL in Oosterhoff type I clusters remain on the ZAHB during their entire lifetimes. In this sense, it is worth noting that the $Z = 0.0005$ case shown in Table 14 and Figures 11 and 13-16 should provide a fairly realistic description of metal-poor Oosterhoff type II clusters with α-elements enhanced by a factor of about three and with [Fe/H] $\simeq -2$—such as M68. However, M68 has an HB type $(B-R)/(B+V+R) = 0.44$ (Walker 1994), whereas $(B-R)/(B+V+R)_{\rm min} = 0.7$ for the $Z = 0.0005$ case (Table 14). Hence it is not possible to successfully model an Oosterhoff type II cluster such as M68 if one requires that all its RRL have evolved from blue ZAHB positions. Again, this is in agreement with similar arguments put forth by Renzini & Fusi Pecci (1988) and Rood & Crocker (1989).

We conclude that, if the Clement et al. (2001) suggestion that NGC 6388 and NGC 6441 are both Oosterhoff type II is confirmed, this will most likely require a revision of the evolutionary interpretation of the Oosterhoff dichotomy, suggesting that there may be different reasons why RRL in Oosterhoff type II globular clusters are brighter than those in Oosterhoff type I globular clusters—evolution away from the blue ZAHB being one such reason, but perhaps not the only one, even for metal-poor clusters such as M68 and M15. If, on the other hand, it should turn out that RRL in all Oosterhoff type II globulars are indeed evolved, then extant evolutionary calculations seriously underestimate the duration of the late stages of HB evolution. The latter is, in fact, a possibility that will have to be seriously considered in future investigations. As well known, there is considerable evidence pointing to redward evolution for RRL in Oosterhoff type II globular clusters beyond that considered in the present analysis—including the RRc-to-RRab number ratios and mean (secular) period change rates (Smith 1995 and references therein). Uncertainties currently

affecting HB models, and which may be relevant when considering this issue, include those directly related to HB evolution and those affecting it indirectly, by means of the properties of RGB models by the time they reach the tip of the RGB. Among the former may be listed the $^{12}C(\alpha,\gamma)^{16}O$ reaction rates, since this reaction dominates over the triple-α reaction at the late stages of HB evolution, and the treatment of "breathing pulses" which occur when He is close to being exhausted in the cores of HB stars (see §2.2.4 in Catelan et al. 2001a for a related discussion and references). Among the latter, most important are those that affect the determination of the size of the He-core mass at the He-flash, M_c. This is because HB stars spend most of their lifetime not on the ZAHB proper, but evolving on "blueward loops" in the HR diagram (see, e.g., Figure 11); the size of these loops is strongly affected by the value of M_c (e.g., Sweigart & Gross 1976). If blue HB stars evolved more directly to the red, instead of spending so much time evolving to the blue along these "blueward loops," HB tracks such as those depicted in Figure 11 would spend much more time in the instability strip, so that HB simulations like those in Figures 14-16 would give rise to larger numbers of RRL. In fact, an increase in M_c was earlier suggested by Castellani & Tornambè (1981) and Catelan (1992) as a possible way to help account for the evolutionary properties of RRL in Oosterhoff type II globulars. The value of M_c is uncertain due to a variety of factors, as extensively discussed by Catelan, de Freitas Pacheco, & Horvath (1996) and Salaris, Cassisi, & Weiss (2002). Particularly noteworthy is the current lack of reliable electron conductive opacities for the physical conditions characterizing the interiors of RGB stars. Outside the canonical framework, the interplay between stellar rotation and the value of M_c has still not been firmly established; it is certainly a possibility that rapidly rotating RGB cores will be able to attain higher masses by the time of the He-flash than non-rotating RGB cores (Mengel & Gross 1976).

Due to these uncertainties, it remains unclear whether the failure of the current generations of HB models to account for the properties of Oosterhoff type II globulars is

fatal to the evolutionary scenario, or whether future improvements in the input physics and in producing realistic models of HB and RGB stars will prove that the evolutionary scenario is indeed the correct explanation. What *is* clear, at present, is that the evolutionary interpretation of the Oosterhoff dichotomy is far from being conclusively settled—and even more so in the cases of NGC 6388 and NGC 6441, whose detailed properties differ in several important respects from those of typical Oosterhoff type II globulars.

6. Summary and Conclusions

The unusual horizontal branch morphology in NGC 6388 is confirmed in this ground-based study. Typical of a metal-rich globular cluster, NGC 6388 contains a strong red component to the horizontal branch. A blue component can also be seen extending through the instability strip, sloping upward in V with decreasing $(B-V)$. This second-parameter effect cannot be explained by age or increased mass loss along the red giant branch (Sweigart & Catelan 1998). It may also be that NGC 6388 has a spread in metallicity, so that the blue component would then be due to a lower metallicity.

The number of known RR Lyrae has been increased to 14. The periods of the RRab stars are found to be unusually long for the metallicity of NGC 6388. In fact, as seen in a period-amplitude diagram comparing NGC 6388 to other globular clusters, the periods for the RRab stars are as long as, if not longer than, those found in Oosterhoff type II clusters. A small number of long period RRc stars were found in NGC 6388, resulting in a smaller than expected gap between the shortest period RRab and longest period RRc stars. Long period RRc stars are uncommon in globular clusters with the exceptions of ω Cen and NGC 6441.

The reddening was determined to be $E(B-V) = 0.40 \pm 0.03$ mag with some differential

reddening for NGC 6388. The mean V magnitude for the horizontal branch from the RR Lyrae was found to be 16.85 ± 0.05 mag leading to a range in distance of 9.0 to 10.3 kpc, depending on the adopted HB absolute magnitude.

Four candidate Population II Cepheids were found in the field of NGC 6388. Although their existence agrees with the extended blue tail in NGC 6388, their likely membership makes NGC 6388 the most metal-rich globular cluster known to contain Population II Cepheids. However, such stars may still be fairly metal-poor, in the case there is an internal metallicity spread in the cluster. The distance of NGC 6388 derived from the Cepheids is 10.6 kpc.

NGC 6388 does not appear to fit in to the typical Oosterhoff classification scheme. The long periods of the RRab in NGC 6388 contradict the trend of increasing period with decreasing metallicity, for a given amplitude. If there is no spread in metallicity in NGC 6388, this implies that the metallicity-luminosity relationship for RR Lyrae is not universal. We provide a detailed discussion, based on theoretical HB models and simulations, of the recent suggestion that NGC 6441—and, by analogy, NGC 6388—can be classified as Oosterhoff type II, also confirming previous difficulties in accounting for the Oosterhoff dichotomy in terms of an evolutionary scenario.

This work has been supported by the National Science Foundation under grants AST 9528080 and AST 9986943. A. V. S. gratefully acknowledges support from NASA Astrophysics Theory Program proposal NRA-99-01-ATP-039.

B. P. would like to thank Peter Stetson for the use of his reduction programs and his assistance in getting them to run properly. Thank you to Nancy Silbermann for sharing her knowledge of the reduction programs. Thank you to Suzanne Hawley and Tim Beers for their insightful comments. Thank you to Brian Sharpee for the use of his spline programs.

We would also like to thank Christine Clement for the use of her Fourier deconvolution program, for providing analytical formulae for her Oosterhoff lines in the period-amplitude diagram, and for useful discussions. We also thank Johanna Jurcsik for her assistance in the preliminary Fourier parameters for the NGC 6441 variables, and Manuela Zoccali for providing number counts along the HBs of NGC 6388 and NGC 6441.

REFERENCES

Alcaino, G. 1981, A&AS, 44, 33

Alcock, C., et al. 1996, AJ. 111, 1146

Armandroff, T. E., & Zinn, R. 1988, AJ, 96, 92

Bingham, E. A., Cacciari, C., Dickens, R. J., & Fusi Pecci, F. 1984, MNRAS, 209, 765

Blanco, V. 1992, AJ, 104, 734

Bono, G., Cassisi, S., Zoccali, M., & Piotto, G. 2001, ApJ, 546, L109

Borissova, J., Ivanov, V. D., & Catelan, M. 2000, IBVS, 4919

Brocato, E., Castellani, V., Scotti, G. A., Saviane, I., Piotto, G., & Ferraro, F. R. 1998, A&A, 335, 929

Butler, D., Dickens, R. J., & Epps, E. 1978, ApJ, 225, 148

Caputo, F. 1981, Ap&SS, 76, 329

Caputo, F., Marconi, M., & Santolamazza, P. 1998, MNRAS, 293, 364

Carney, B. W. 1996, PASP, 108, 900

Carney, B. W., Storm, J., & Williams, C. 1993, PASP, 105, 294

Carretta, E., Cacciari, C. Ferraro, F. R., Fusi Pecci, F., & Tessicini, G. 1998, MNRAS, 298, 1005

Castellani, V., & Tornambè, A. 1981, A&A, 96, 20

Catelan, M. 1992, A&A, 261, 457

Catelan, M. 1993, A&AS, 98, 547

Catelan, M., Borissova, J., Sweigart, A. V., & Spassova, N. 1998, ApJ, 494, 265

Catelan, M., de Freitas Pacheco, J. A., & Horvath, J. E. 1996, ApJ, 461, 231

Catelan, M., Bellazzini, M., Landsman, W. B., Ferraro, F. R., Fusi Pecci, F., & Galleti, S. 2001a, AJ, 122, 3171

Catelan, M., Ferraro, F. R., & Rood, R. T. 2001b, ApJ, 560, 970

Clement, C. 2000, in The Impact of Large-Scale Surveys on Pulsating Star Research, ed. L. Szabados & D. W. Kurtz (San Francisco: ASP), 266

Clement, C., et al. 2001, AJ, 122, 2587

Clement, C. Dickens, R. J., & Bingham, E. E. 1979, AJ, 84, 217

Clement, C., & Rowe, J. 2000, AJ, 120, 2579

Clement, C., & Shelton, I. 1997, AJ, 113, 1711

Clement, C., & Shelton, I. 1999, ApJ, 515, L85

Cohn, H. N., Lugger, P. M., Grindlay, J. E., & Edmonds, P. D. 2002, ApJ, in press (astro-ph/0202059)

Edmonds, P. D., Grindlay, J. E., Cohn, H., & Lugger, P. 2001, ApJ, 547, 829

Fusi Pecci, F., Ferraro, F. R., Crocker, D. A., Rood, R. T., & Buonanno, R. 1990, A&A, 238, 95

Gingold, R. A. 1976, ApJ, 204, 116

Graham, J. A. 1982, PASP, 94, 244

Harris, H. C. 1985, in Cepheids: Theory and Observations, ed. E. R. Madore (London: Cambridge University Press), 232

Harris, W. E. 1996, AJ, 112, 1487

Hazen, M. L., & Hesser, B. H. 1986, AJ, 92, 1094

Jurcsik, J. 1998, A&A, 333, 571

Jurcsik, J., & Kovács, G. 1996, A&A, 312, 111

Jurcsik, J., & Kovács, G. 1999, New Astronomy Reviews, 43, 463

Kaluzny, J., Hilditch, R. W., Clement, C., & Rucinski, S. M. 1998, MNRAS, 296, 347

Kaluzny, J., Olech, A., Thompson, I., Pych, W., Krzeminski, W., & Schwarzenberg-Cerny, A. 2000, A&AS, 143, 215

Kholopov, P. N. 1985, General Catalogue of Variable Stars (4th ed.; Moscow: Nauka)

Kovács, G. 1998, in A Half Century of Stellar Pulsation Interpretation: A Tribute to Arthur N. Cox, ed. P. A. Bradley & J. A. Buzik (San Francisco: ASP), 52

Kovács, G., & Jurcsik, J. 1997, A&A, 322, 218

Landolt, A. U. 1992, AJ, 104, 340

Layden, A. C., Ritter, L. A., Welch, D. L., & Webb, T. M. A. 1999, AJ, 117, 1313

Layden, A. C., & Sarajedini, A. 2000, AJ, 119, 1760

Lee, Y.-W. 1990, ApJ, 363, 159

Lee, J.-W., & Carney, B. W. 1999, AJ, 118, 1373

Lee, Y.-W., Demarque, P., & Zinn, R. 1990, ApJ, 350, 155

Lloyd Evans, T., & Menzies, J. W. 1973, in Variable Stars in Globular Clusters and in Related Systems, ed. J. D. Fernie (Boston: Reidel), 151

LLoyd Evans, T., & Menzies, J. W. 1977, MNRAS, 178, 163

McNamara, D. H., 1995, AJ, 109, 2134

Mengel, J. G. 1973, in Variable Stars in Globular Clusters and in Related Systems, ed. J. D. Fernei (Boston: Reidel), 214

Mengel, J. G., & Gross, P. G. 1976, Ap&SS, 41, 407

Mohler, S. 2001, PASP, 113, 1162

Nemec, J. M., Nemec, A. F. L., & Lutz, T. E. 1994, AJ, 108, 222

Pancino, E., Ferraro, F. R., Bellazzini, M., Piotto, G., & Zoccali, M. 2000, ApJ, 534, L83

Petersen, J. O. 1986, A&A, 170, 59

Piotto, G., et al. 1997, in Advances in Stellar Evolution, ed. R. T. Rood & A. Renzini (Cambridge: Cambridge University Press), 84

Piotto, G., et al. 1999, AJ, 118, 1727

Pritzl, B., Smith, H. A., Catelan, M., & Sweigart, A. V. 2000, ApJ, 530, L41

Pritzl, B., Smith, H. A., Catelan, M., & Sweigart, A. V. 2001, 122, 2600

Raimondo, G., Castellani, V., Cassisi, S., Brocato, E., & Piotto, G. 2002, ApJ, in press (astro-ph/0201123)

Ree, C. H., Yoon, S.-J., Rey, S.-C., Lee, Y.-W. 2002, in Omega Centauri: A Unique Window Into Astrophysics, ed. F. van Leeuwen, G. Piotto, & J. Hughes (Cambridge: Cambridge University Press), in press (astro-ph/0110689)

Reed, B. C., Hesser, J. E., Shawl, S. J. 1988, PASP, 100, 545

Reimers, D. 1975, in Mem. Soc. R. Sci. Liège 6 Sér., 8, 369

Renzini, A., & Fusi Pecci, F. 1988, ARA&A, 26, 199

Rich, R. M., Minniti, D., & Liebert, J. 1993, ApJ, 406, 489

Rich, R. M., et al. 1997, ApJ, 484, L25

Rood, R. T. 1973, ApJ, 184, 815

Rood, R. T., & Crocker, D. A. 1989, in IAU Colloq. 111, The Use of Pulsating Stars in Fundamental Problems of Astronomy, ed. E. G. Schmidt (Cambridge: Cambridge University Press), 103

Salaris, M., Cassisi, S., & Weiss, A. 2002, PASP, in press (astro-ph/0201387)

Sandage, A. 1990, ApJ, 350, 603

Sandage, A., & Wildey, R. 1967, ApJ, 150, 469

Schlegel, D. J., Finkbeiner, D. P., & Davis, M. 1998, ApJ, 500, 525

Silbermann, N. A., & Smith, H. A., 1995, AJ, 110, 704

Silbermann, N. A., Smith, H. A., Bolte, M., & Hazen, M. L. 1994, AJ, 107, 1764

Simon, N. R., & Clement, C. 1993a, ApJ, 410, 526

Simon, N. R., & Clement, C. 1993b, in IAU Colloq. 139, New Perspectives on Stellar Pulsation and Pulsating Variable Stars, ed. J. M. Nemec & J. M. Matthews (Cambridge: Cambridge University Press), 315

Simon, N. R., & Teays, T. J. 1982, ApJ, 261, 586

Smith, H. A. 1995, RR Lyrae Stars (Cambridge: Cambridge University Press)

Smith H. A., & Wehlau, A. 1985, ApJ, 298, 572

Stellingwerf, R. F., Gautschy, A., & Dickens, R. J. 1987, ApJ, 313, L75

Sweigart, A. V. 1978, in The HR Diagram, ed. A. G. Davis Philip & D. S. Hayes (Dordrecht: Reidel), 333

Sweigart, A. V. 1999, in Spectrophotometric Dating of Stars and Galaxies, ASP Conf. Ser. Vol. 192, ed. I. Hubeny, S. Heap, & R. Cornett (San Francisco: ASP), 239

Sweigart, A. V. 2002, in Highlights of Astronomy, Vol. 12, in press (astro-ph/0103133)

Sweigart, A. V., & Catelan, M. 1998, ApJ, 501, L63

Sweigart, A. V. & Gross, P. G. 1976, ApJS, 32, 367

Sweigart, A. V., Renzini, A., & Tornambè, A. 1987, ApJ, 312, 762

van Albada, T. S., & Baker, N. 1973, ApJ, 185, 477

van den Bergh, S. 1967, PASP, 79, 460

Walker, A. R. 1994, AJ, 108, 555

Walker, A. R. 2000, in The Impact of Large-Scale Surveys on Pulsating Star Research, ed. L. Szabados & D. W. Kurtz (San Francisco: ASP), 165

Walker, A. R., & Nemec, J. M. 1996, AJ, 112, 2026

Wallerstein, G. W. 1970, ApJ, 160, 345

Zinn, R. 1980, ApJS, 42, 19

Zoccali, M., Cassisi, S., Bono, G., Piotto, G., Rich, R. M., & Djorgovski, S. G. 2000, ApJ, 538, 289

Zoccali, M., Cassisi, S., Piotto, G., Bono, G., & Salaris, M. 1999, ApJ, 518, L49

This manuscript was prepared with the AAS LaTeX macros v5.0.

Fig. 1.— Color-magnitude diagrams for the NGC 6388 stars located in the complete field of view (a), out to a radius of 1.7 arcmin (b) and 2.7 arcmin (c) from the cluster center, and outside a radius of 6.5 arcmin from the cluster center (d).

Fig. 2.— Finding charts for the NGC 6388 variable stars. North is down and east is left.

Fig. 3.— Color-magnitude diagram for the fundamental mode RR Lyrae (filled circles), first overtone RR Lyrae (filled squares), suspected RR Lyrae (filled triangles), and Population II Cepheids (five-pointed stars) in the field of NGC 6388.

Fig. 4.— V and B light curves of NGC 6388 variable stars.

Fig. 5.— Fourier parameter plot using A_{21} vs. ϕ_{21} to show the distinction between RR Lyrae types in NGC 6388.

Fig. 6.— Period-amplitude diagram for NGC 6388 in V and B showing fundamental mode RR Lyrae (filled squares) and first overtone RR Lyrae (open squares). The dashed and solid lines represents the Oosterhoff types I and II lines, respectively, as given by Clement (2000; private communication).

Fig. 7.— Nightly light curves for V35. Night 4 appears to have a different amplitude and phase than the other nights.

Fig. 8.— Period distribution histogram for the RR Lyrae in NGC 6388. The dark area is occupied by c-type RR Lyrae. The light area is occupied by ab-type RR Lyrae. Only RR Lyrae with certain classification are included.

Fig. 9.— Period-amplitude diagram for the ab-type RR Lyrae of NGC 6388 (open circles) as compared to field RR Lyrae of [Fe/H] ≥ -0.8 (asterisks), V9 in 47 Tucanae (open star), M3 (open boxes), M15 (filled stars), and M68 (filled triangles). The filled circles represent the RRab stars in NGC 6441 from Pritzl et al. (2001). The boxed area, taken from Figure 9

of Layden et al. (1999), denotes the region predicted by Sweigart & Catelan (1998) where the RR Lyrae should be located according to a helium-mixing scenario.

Fig. 10.— Period-amplitude diagram for the c-type RR Lyrae in ω Cen in comparison to those found in NGC 6388 and NGC 6441.

Fig. 11.— Evolutionary tracks for blue HB stars with heavy-element abundances Z of 0.0005, 0.001, 0.002 and 0.006. In each panel, label "a" identifies the HB track corresponding to the $M_{\rm HB,ev}$ value shown in Table 14. Label "b" indicates the HB track corresponding to a ZAHB position with $(B-V)_0 = 0$, which is the color of the peak of the blue HB distribution in NGC 6441; and label "c" corresponds to a ZAHB position with $(B-V)_0 = -0.1$, which is the color of the peak of the blue HB distribution in NGC 6388. Each track is plotted as a series of points separated by a time interval of 200,000 yr in order to indicate the rate of evolution. The two thin vertical lines along each track mark the blue and red edges of the instability strip. The solid curves give the ZAHB locus for each metallicity. Note the sharp drop in the time spent within the instability strip between tracks "a" and "c."

Fig. 12.— Number ratio V/B of variables to blue HB stars predicted by HB evolutionary tracks with heavy-element abundances Z of 0.0005, 0.001, 0.002 and 0.006. The ordinate gives the ratio of the time spend within the instability strip to the time spent blueward of the instability strip for blue HB tracks that only enter the instability strip during the final evolution back to the asymptotic giant branch. The abscissa gives the time-averaged value of log $T_{\rm eff}$ over the part of the HB track blueward of the instability strip. The low temperature end of each curve is set by the mass $M_{\rm HB,ev}$ (see text). Note the sharp decline in the fraction of the HB lifetime spent within the instability strip as the mean HB effective temperature increases.

Fig. 13.— Location of the HB evolutionary tracks from Figure 11 in the period-temperature

plane. Periods were computed from the pulsation equation of van Albada & Baker (1971). Only the part of the tracks within the instability strip are plotted. Each track is labeled at the blue edge of the instability strip. As in Figure 11 the tracks are plotted as a series of points separated by a time interval of 200,000 yr. The "c" tracks evolve so rapidly that they contain only 1 or 2 points within the instability strip. A finer time resolution would show that the "c" tracks run approximately parallel to the "a " and "b" tracks. For comparison the period-temperature locus of the "a" track with $Z = 0.006$ is plotted as a thin line in the three lower metallicity panels. Note that corresponding tracks in the panels for $Z \leq 0.002$ have very similar loci. In contrast, the tracks for $Z = 0.006$ are shifted towards shorter periods.

Fig. 14.— Synthetic HB simulations of Oosterhoff type II globular clusters with all RR Lyrae evolved away from a position on the blue ZAHB. RR Lyrae are indicated by encircled dots. From upper left to lower right, progressively bluer HB types are shown. The input values of the mean ZAHB mass and corresponding dispersion are indicated in each panel. Note that, even in the upper left panel, the HB morphology does not get redder than $(B-R)/(B+V+R) = +0.89$, which is much bluer than Oosterhoff type II globulars such as M15 and M68.

Fig. 15.— As in Figure 14, but zooming on the distributions around the RR Lyrae level. Note the increasing concentration of the RR Lyrae distribution towards its lower envelope (which is well approximated by line "a" in the upper left panel of Figure 11) as the HB gets redder; the presence of intrinsic scatter in all the simulations; and the decrease in the number of variables as the HB gets bluer.

Fig. 16.— As in Figure 15, but showing the $\log P - \log T_{\rm eff}$ distribution. A line has been drawn on all panels that corresponds to the lower envelope of the higher-$\langle M_{\rm HB} \rangle$ distribution (which is well approximated by line "a" in the upper left panel of Figure 13). The mean shift in periods (at fixed $T_{\rm eff}$) for each of the simulations is indicated, as is the corresponding

standard deviation. Note the shift towards longer mean periods and the increase in the intrinsic scatter as the HB gets bluer.

Table 1. Mean Differences in Photometry

Reference	ΔV	ΔB
Alcaino	0.03±0.02	0.02±0.03
Silbermann et al.	0.007±0.008	-0.004±0.008
HST	0.035±0.007	0.025±0.010

Note. — difference = reference magnitude - magnitude in present study

Table 2. Locations of Variable Stars

ID	X	Y	$\Delta\alpha$	$\Delta\delta$
V4	1560.0	999.9	-192.2	26.0
V12	1228.2	1067.0	-60.7	-0.8
V14	1532.5	1858.0	-184.0	-310.9
V16	1743.4	447.1	-263.2	243.2
V17	1170.8	1129.4	-38.1	-25.4
V18	1147.5	949.0	-28.3	45.4
V20	938.0	965.0	54.9	38.8
V21	911.2	722.6	66.3	133.9
V22	901.0	1076.3	69.2	-4.9
V23	1528.6	1016.9	-179.8	19.3
V26	793.3	1228.3	111.5	-64.7
V27	923.4	1106.7	60.2	-16.8
V28	1014.8	1194.5	23.7	-51.1
V29	1124.4	1052.1	-19.4	4.9
V30	951.3	1089.8	49.2	-10.1
V31	768.4	823.1	122.7	94.3
V32	1170.9	1138.8	-38.1	-29.1
V33	907.3	854.0	67.4	82.4
V34	1562.0	1184.7	-193.6	-46.6
V35	898.0	535.9	72.1	207.2
V36	1004.7	1025.3	28.2	15.3
V37	1072.7	1127.3	0.9	-24.7
V38	1088.9	1638.4	-7.2	-225.3
V39	815.2	9.6	106.7	413.7
V40	904.7	525.6	69.5	211.3

Table 2—Continued

ID	X	Y	$\Delta\alpha$	$\Delta\delta$
V41	62.1	332.7	404.6	285.8
V42	456.0	620.1	247.3	173.6
V43	1467.1	1010.7	-155.3	21.6
V44	1607.4	1151.7	-211.5	-33.6
V45	649.7	341.7	171.3	283.1
V46	1283.6	1158.4	-82.9	-36.6
V47	359.0	1523.1	283.0	-181.0
V48	1004.9	1030.6	28.1	13.2
V49	1048.9	1168.0	10.2	-40.7
V50	1130.0	1006.1	-21.5	23.0
V51	1006.9	1134.3	27.0	-27.5
V52	1530.4	1564.3	-182.2	-195.6
V53	1278.0	973.1	-80.1	36.1
V54	1589.2	1115.1	-204.1	-19.2
V55	1037.2	1229.8	14.7	-65.0
V56	1130.4	1097.4	-22.1	-13.8
V57	1821.4	571.7	-294.6	194.4

Table 3. Mean Properties of RR Lyrae

ID	Period	$\langle V \rangle$	$(B-V)_{\rm mag}$	A_V	A_B	Comments
V16	0.251	16.895	0.538	0.26	0.31	c
V17	0.611	16.525	0.687	0.85	1.15	ab
V20	0.467	16.787	0.447	0.36	0.46	c
V21	0.814	17.030	0.760	0.87	1.15	ab
V22	0.587	16.858	0.706	1.12	1.57	ab
V23	0.338	16.893	0.520	0.48	0.65	c
V26	0.239	17.403	0.522	0.38	0.51	c
V27	0.365	16.953	0.585	0.46	0.67	c
V28	0.840	16.820	0.824	0.80	1.05	ab
V30	0.951	16.766	0.863	···	···	ab?
V31	0.341	17.031	0.550	0.52	0.70	c
V32	0.522	16.578	0.598	0.42	0.52	c, S1
V33	0.558	16.747	0.712	0.29	0.42	c
V34	0.286	17.409	0.544	0.36	0.50	c
V35	0.300	17.041	0.525	0.18	0.23	c
V44	0.080	18.082	0.533	0.50	0.67	δ Scuti
V48	0.355	16.574	0.421	···	0.34	c?
V49	0.384	16.925	0.628	0.52	0.65	c?, S2
V50	0.364	16.898	0.965	0.54	···	c?
V51	0.397	16.604	0.733	0.34	0.48	c?

Table 3—Continued

ID	Period	$\langle V \rangle$	$(B-V)_{\rm mag}$	A_V	A_B	Comments
V52	0.387	16.686	0.661	0.23	0.55	c?
V53	0.986	16.868	0.773	···	···	ab?, S3
V55	0.489	16.795	0.649	···	···	c?
V56	0.552	16.825	0.687	···	···	c?

Table 4. Photometry of the Variable Stars (V)

	V16		V17	
HJD-2450000	V	σ_V	V	σ_V
966.266	16.787	0.018	16.365	0.064
959.172	16.970	0.017	16.724	0.035
959.237	16.791	0.019	16.782	0.025
960.112	17.001	0.018	16.277	0.018
960.212	16.837	0.018	16.532	0.033
961.301	16.829	0.018	16.219	0.028
961.335	16.937	0.018	16.272	0.022
961.367	17.008	0.019	16.406	0.025
962.065	16.850	0.017	16.565	0.036
962.117	16.988	0.032	16.544	0.053
962.155	17.029	0.017	16.629	0.074
962.216	16.845	0.021	16.747	0.071
962.257	16.760	0.018	16.789	0.059
962.294	16.797	0.019	16.760	0.113
962.330	16.883	0.022	16.879	0.060
965.076	16.844	0.018	16.473	0.024
965.114	16.955	0.018	16.532	0.048
965.146	17.014	0.021	16.558	0.065
965.183	17.016	0.018	16.595	0.047
965.216	16.926	0.016	16.660	0.036
965.248	16.801	0.016	16.716	0.039
965.280	16.775	0.018	16.733	0.053
965.312	16.820	0.016	16.753	0.058

Table 4—Continued

	V16		V17	
HJD-2450000	V	σ_V	V	σ_V
965.346	16.901	0.019	16.783	0.063
966.062	16.804	0.018	16.881	0.058
966.094	16.878	0.017	16.600	0.045
966.135	16.982	0.017	16.011	0.055
966.167	17.026	0.018	16.056	0.060
966.203	16.984	0.016	16.185	0.060
966.233	16.867	0.016	16.291	0.065
966.327	16.839	0.019	16.516	0.075
967.050	16.776	0.020	16.674	0.043
967.082	16.843	0.018	16.715	0.065
967.114	16.921	0.018	16.756	0.060
967.146	16.996	0.017	16.731	0.089
967.188	17.018	0.016	16.820	0.055
967.243	16.848	0.018	16.886	0.055
967.276	16.774	0.016	16.862	0.069
967.308	16.788	0.016	16.696	0.051
967.345	16.869	0.018	16.084	0.070
968.056	16.786	0.018	16.295	0.026
968.089	16.840	0.017	16.412	0.032
968.122	16.921	0.017	16.498	0.032
968.163	17.009	0.018	16.532	0.024
968.195	17.014	0.017	16.598	0.031
968.236	16.889	0.017	16.614	0.029

Table 4—Continued

	V16		V17	
HJD-2450000	V	σ_V	V	σ_V
968.274	16.779	0.017	16.662	0.031
968.307	16.775	0.017	16.702	0.021

Note. — The complete version of this table is in the electronic edition of the Journal. The printed edition contains only a sample.

Table 5. Photometry of the Variable Stars (B)

	V16		V17	
HJD-2450000	B	σ_B	B	σ_B
966.274	17.287	0.012	17.103	0.072
959.183	17.491	0.011	17.474	0.040
959.246	17.299	0.014	17.541	0.031
960.120	17.584	0.013	16.897	0.017
961.309	17.377	0.008	16.709	0.059
961.343	17.509	0.010	16.847	0.031
962.057	17.386	0.014	17.249	0.031
962.097	17.473	0.012	17.274	0.039
962.147	17.598	0.011	17.326	0.076
962.188	17.520	0.007	17.481	0.078
962.205	17.437	0.006	17.525	0.073
962.228	17.327	0.007	17.535	0.066
962.265	17.260	0.011	17.581	0.073
962.302	17.343	0.017	17.675	0.092
962.337	17.450	0.020	17.649	0.057
965.068	17.365	0.013	17.072	0.018
965.106	17.487	0.014	17.201	0.033
965.138	17.582	0.014	17.283	0.068
965.191	17.564	0.008	17.338	0.037
965.223	17.432	0.007	17.413	0.039
965.255	17.288	0.007	17.544	0.061
965.288	17.296	0.008	17.523	0.055
965.320	17.354	0.010	17.550	0.055

Table 5—Continued

	V16		V17	
HJD-2450000	B	σ_B	B	σ_B
965.354	17.471	0.017	17.626	0.060
966.054	17.296	0.017	17.679	0.058
966.086	17.394	0.011	17.404	0.051
966.127	17.513	0.011	16.512	0.048
966.159	17.582	0.011	16.517	0.061
966.195	17.563	0.007	16.698	0.055
966.241	17.355	0.007	16.924	0.060
966.334	17.388	0.013	17.277	0.068
967.058	17.281	0.018	17.467	0.059
967.090	17.381	0.018	17.542	0.073
967.121	17.483	0.011	17.564	0.068
967.154	17.571	0.008	17.553	0.070
967.195	17.578	0.007	17.623	0.073
967.235	17.402	0.008	17.634	0.051
967.268	17.298	0.007	17.664	0.063
967.300	17.281	0.011	17.507	0.050
967.337	17.377	0.012	16.814	0.054
968.046	17.276	0.017	16.804	0.030
968.081	17.345	0.011	16.966	0.024
968.115	17.443	0.008	17.107	0.025
968.155	17.576	0.011	17.217	0.019
968.187	17.590	0.010	17.263	0.021
968.249	17.364	0.007	17.357	0.025

Table 5—Continued

	V16		V17	
HJD-2450000	B	σ_B	B	σ_B
968.282	17.281	0.007	17.399	0.020
968.315	17.306	0.007	17.470	0.024

Note. — The complete version of this table is in the electronic edition of the Journal. The printed edition contains only a sample.

Table 6. Fourier Coefficients

ID	A_1	A_{21}	A_{31}	A_{41}	ϕ_{21}	ϕ_{31}	ϕ_{41}	D_m
V16	0.128	0.094	0.031	0.012	4.760	3.216±0.374	1.909	···
V17	0.295	0.583	0.360	0.196	4.294	2.222±0.068	0.477	5.35
V20	0.180	0.094	0.092	0.050	2.430	5.393±0.347	3.854	···
V21	0.332	0.456	0.191	0.098	4.577	2.879±0.092	1.068	9.01
V22	0.391	0.544	0.337	0.203	4.295	2.196±0.035	0.524	3.10
V23	0.236	0.082	0.035	0.071	3.968	4.390±0.323	2.982	···
V26	0.197	0.128	0.030	0.030	4.624	2.669±0.552	2.585	···
V27	0.234	0.068	0.042	0.048	4.673	5.496±0.506	3.332	···
V28	0.331	0.397	0.133	0.081	4.592	2.973±0.117	1.429	13.17
V31	0.257	0.083	0.055	0.055	4.044	5.082±0.182	3.207	···
V32	0.187	0.218	0.142	0.111	3.377	0.206±0.260	4.277	···
V33	0.132	0.214	0.130	0.027	3.229	0.674±0.188	5.040	···
V34	0.187	0.130	0.085	0.056	4.234	3.017±0.173	2.268	···
V35	0.093	0.037	0.020	0.026	4.340	5.924±0.859	1.672	···
V38	0.035	4.357	0.690	1.591	4.265	3.395±0.306	2.306	···
V39	0.043	2.174	0.526	0.311	5.549	5.040±0.264	4.836	···
V40	0.040	3.943	0.398	0.918	0.034	5.814±0.520	6.276	···
V41	0.285	1.722	1.946	1.789	1.248	2.675±0.055	4.099	···
V42	0.057	1.400	1.314	0.708	0.923	0.667±0.220	1.317	···
V43	20.19	2.451	0.693	1.397	0.010	0.024±0.001	0.017	···
V44	0.215	0.370	0.150	0.094	4.029	1.673±0.140	5.688	···
V48	0.152	0.070	0.157	0.067	4.334	4.345±0.594	3.766	···
V49	0.234	0.054	0.097	0.109	3.291	6.002±0.422	3.480	···
V50	0.242	0.036	0.116	0.126	4.355	5.997±0.392	4.553	···
V51	0.174	0.077	0.106	0.053	2.772	5.139±0.291	4.591	···

Table 6—Continued

ID	A_1	A_{21}	A_{31}	A_{41}	ϕ_{21}	ϕ_{31}	ϕ_{41}	D_m
V52	0.144	0.111	0.205	0.286	4.188	3.479±1.458	3.541	···
V53	5.838	0.621	0.264	0.402	0.179	3.366±1.186	3.655	···
V54	0.067	4.421	0.498	0.974	0.319	1.314±0.675	0.860	···
V55	0.098	0.577	0.762	0.758	1.511	4.910±0.192	2.133	···
V56	0.171	0.054	0.236	0.095	5.967	1.148±0.352	0.170	···
V57	0.073	4.016	0.227	1.402	0.365	0.296±0.419	0.847	···

Table 7. Reddening Determinations

ID	$E(B-V)$
V17	0.365
V21	0.388
V22	0.405
V28	0.431

Table 8. Mean Properties of Cepheid Variables

ID	Period	$\langle V \rangle$	$(B-V)_{\rm mag}$	A_V	A_B
V18	2.89	15.616	0.975	0.77	1.20
V29	1.88	···	···	···	1.05
V36	3.10	15.558	0.850	1.05	1.45
V37	10.0	14.707	1.173	···	···

Table 9. Mean Properties of Binary Stars

ID	Period	$\langle V \rangle$	$(B-V)_{\rm mag}$	A_V	A_B	Comments
V14	2.16	16.179	0.511	1.30	1.30	Detached
V38	0.412	18.270	1.092	0.46	0.56	Contact
V39	0.537	17.996	0.751	0.28	0.30	Contact
V40	0.311	18.806	1.106	0.39	···	Contact
V41	1.71	17.364	0.656	2.20	2.80	Detached
V42	1.82	15.724	0.251	0.48	0.52	Detached
V43	2.02	19.606	0.800	1.22	1.50	Detached
V54	0.366	19.447	0.872	0.67	0.72	Contact
V57	0.278	19.116	1.082	0.80	0.80	Contact

Table 10. Cluster properties

Cluster	Type	[Fe/H]	$\langle P_{ab} \rangle$	$\langle P_c \rangle$	N_c/N_{RR}
M3	Oo I	−1.6	0.56	0.32	0.16
M15	Oo II	−2.2	0.64	0.38	0.48
NGC 6388	?	−0.6	0.71	0.36	0.71
NGC 6441	?	−0.5	0.75	0.38	0.31

Table 11. RRc Parameters

ID	$M/M_\odot$	$\log(L/L_\odot)$	$T_{\rm eff}$	M_V
V16	0.53	1.60	7583	0.87
V23	0.46	1.66	7352	0.76
V31	0.39	1.63	7424	0.76
V34	0.54	1.58	7621	0.87
Mean	0.48±0.07	1.62±0.04	7495±128	0.82±0.06

Table 12. RRab Parameters

ID	$M/M_\odot$	$\log(L/L_\odot)$	$\log T_{\rm eff}$	M_V	[Fe/H]
V17	0.55	1.67	3.82	0.78	–1.12
V21	0.51	1.70	3.81	0.55	–1.33
V22	0.54	1.64	3.83	0.77	–1.02
V28	0.57	1.73	3.80	0.52	–1.35
Mean	0.56±0.03	1.69±0.04	3.82±0.01	0.66±0.14	–1.21±0.16

Table 13. Population II Cepheid Distance Estimates

ID	M_V	M_B	$m_{0,V}$	$m_{0,B}$	d_V	d_B
V18	–0.79	–0.37	14.336	14.951	10.6	11.6
V29	–0.49	–0.12	···	14.395	···	8.0
V36	–0.84	–0.41	14.278	14.768	10.6	10.9
V37	–1.11	–0.37	13.427	14.240	8.1	8.4

Table 14. Reddest Possible HB Morphology of an Oosterhoff Type II Cluster

Z	$M_{\rm HB,ev}$	$(B-R)/(B+V+R)_{\rm min}$	$V/(B+V+R)_{\rm max}$	$B/(B+V+R)_{\rm min}$
0.0005	0.6668	0.729	0.193	0.768
0.001	0.6313	0.823	0.127	0.848
0.002	0.6042	0.839	0.121	0.859
0.006	0.5691	0.740	0.218	0.761

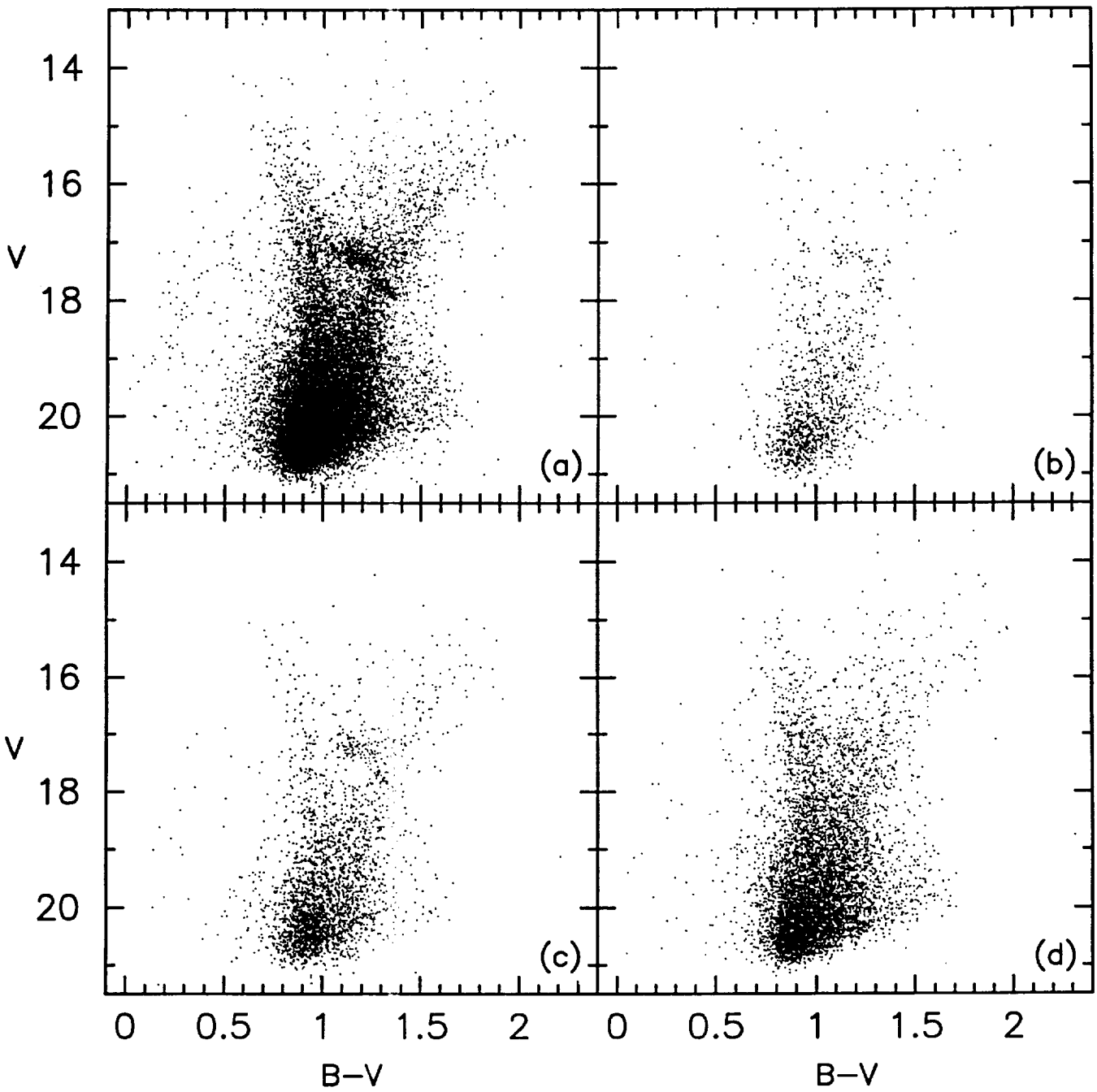

Figure 1

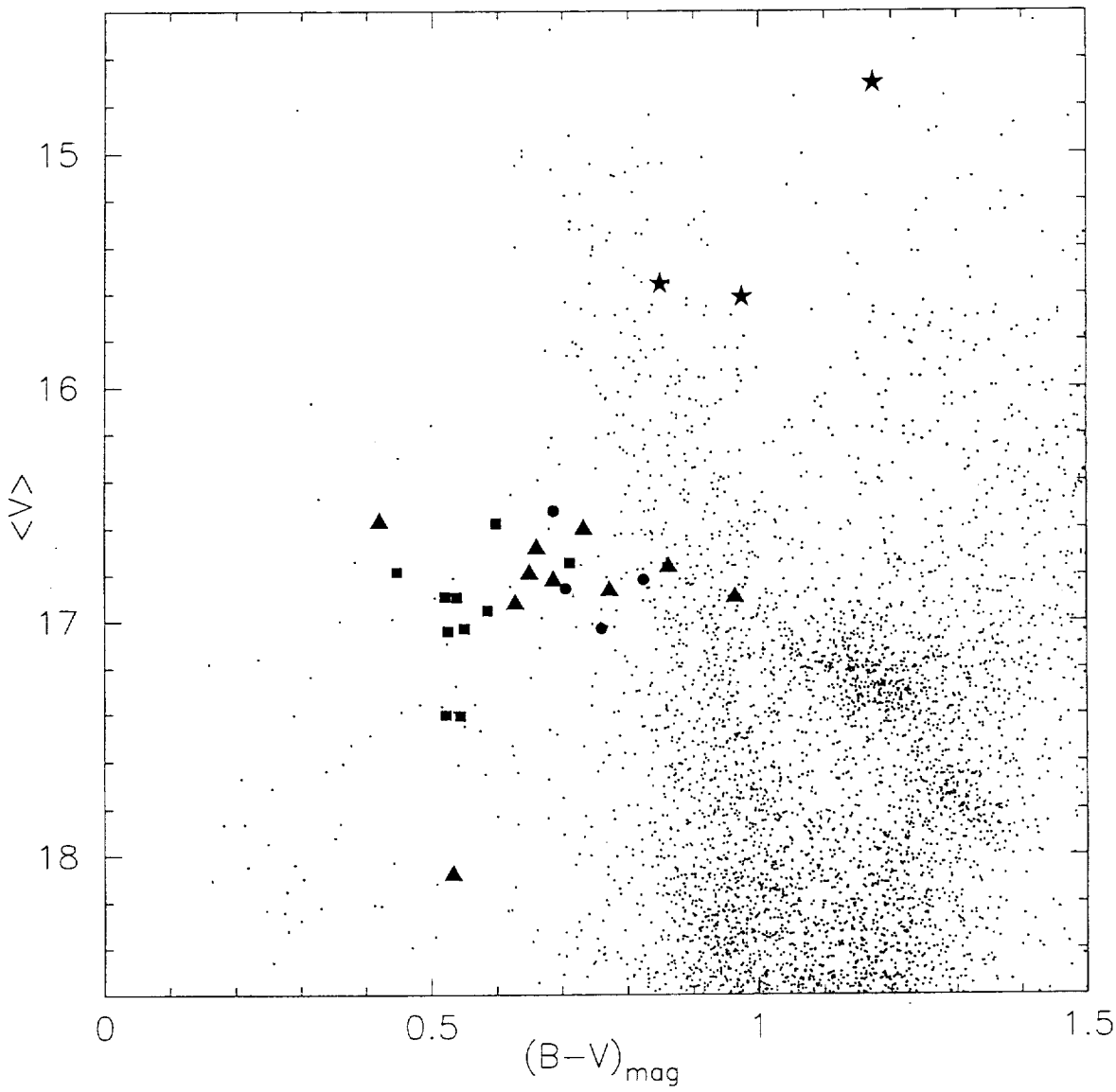

Figure 3

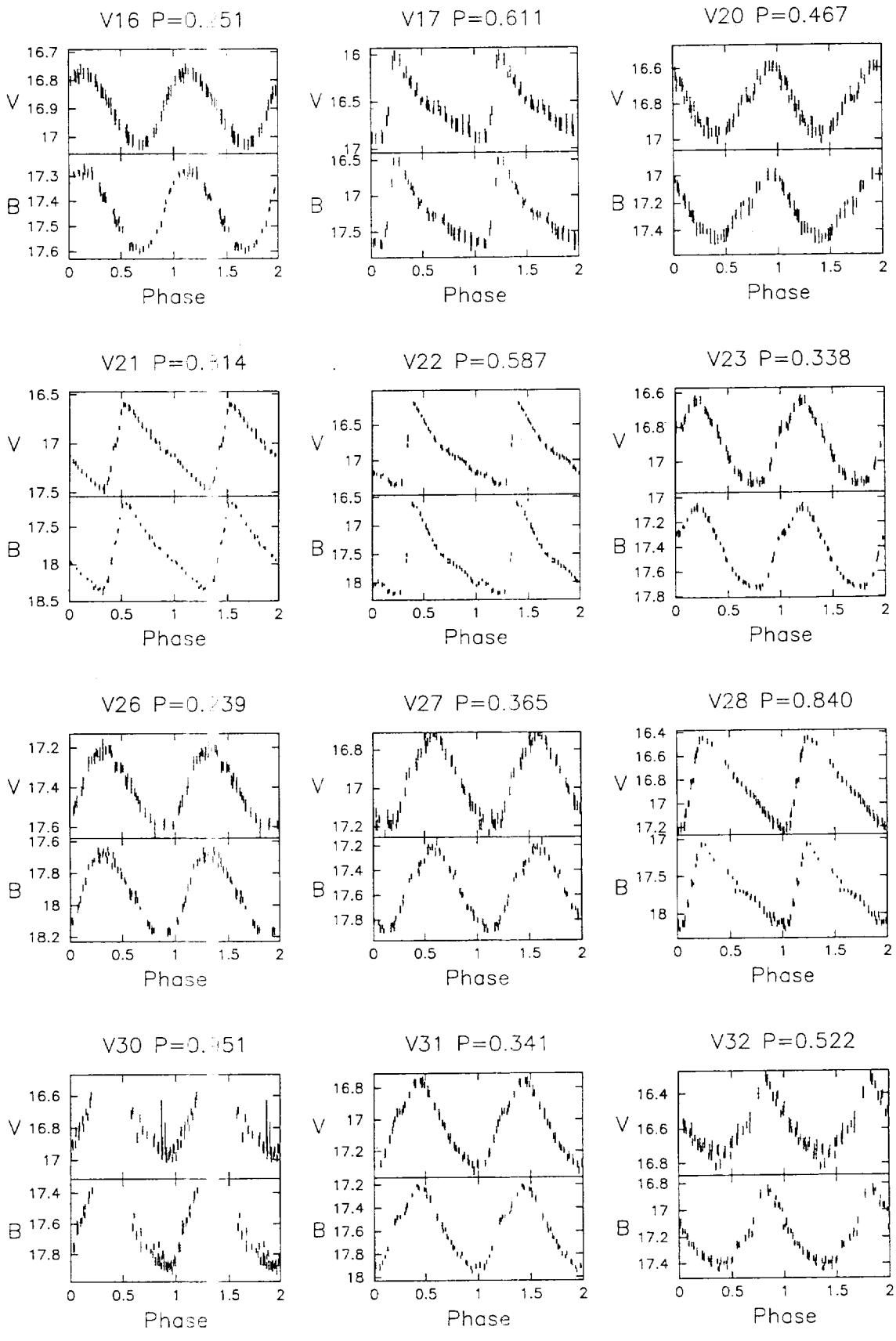
V16 P=0.351
V17 P=0.611
V20 P=0.467
V21 P=0.314
V22 P=0.587
V23 P=0.338
V26 P=0.239
V27 P=0.365
V28 P=0.840
V30 P=0.351
V31 P=0.341
V32 P=0.522
V
B
Phase

Figure 4-a

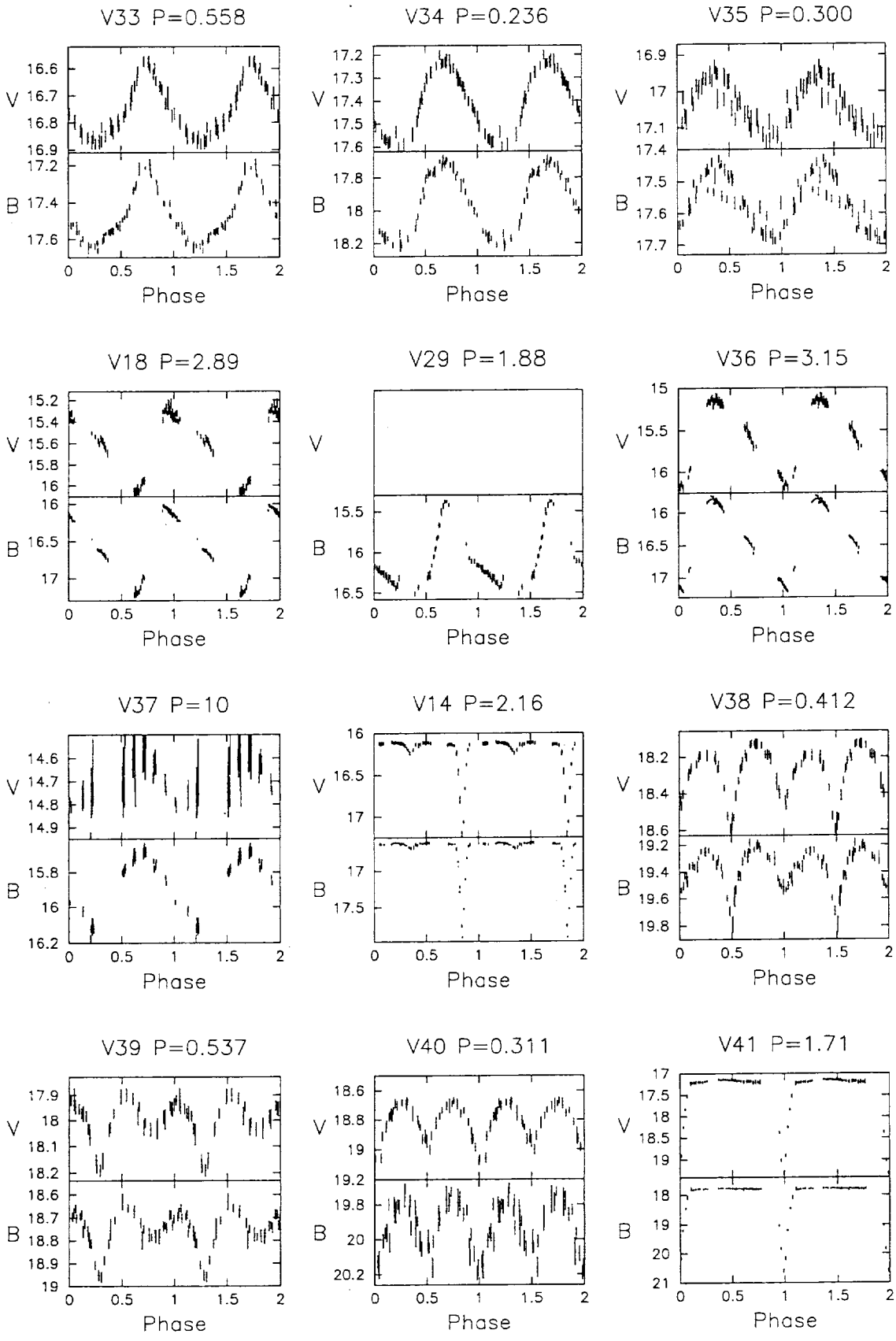
V33 P=0.558
V34 P=0.236
V35 P=0.300
V18 P=2.89
V29 P=1.88
V36 P=3.15
V37 P=10
V14 P=2.16
V38 P=0.412
V39 P=0.537
V40 P=0.311
V41 P=1.71
V
B
Phase

Figure 46

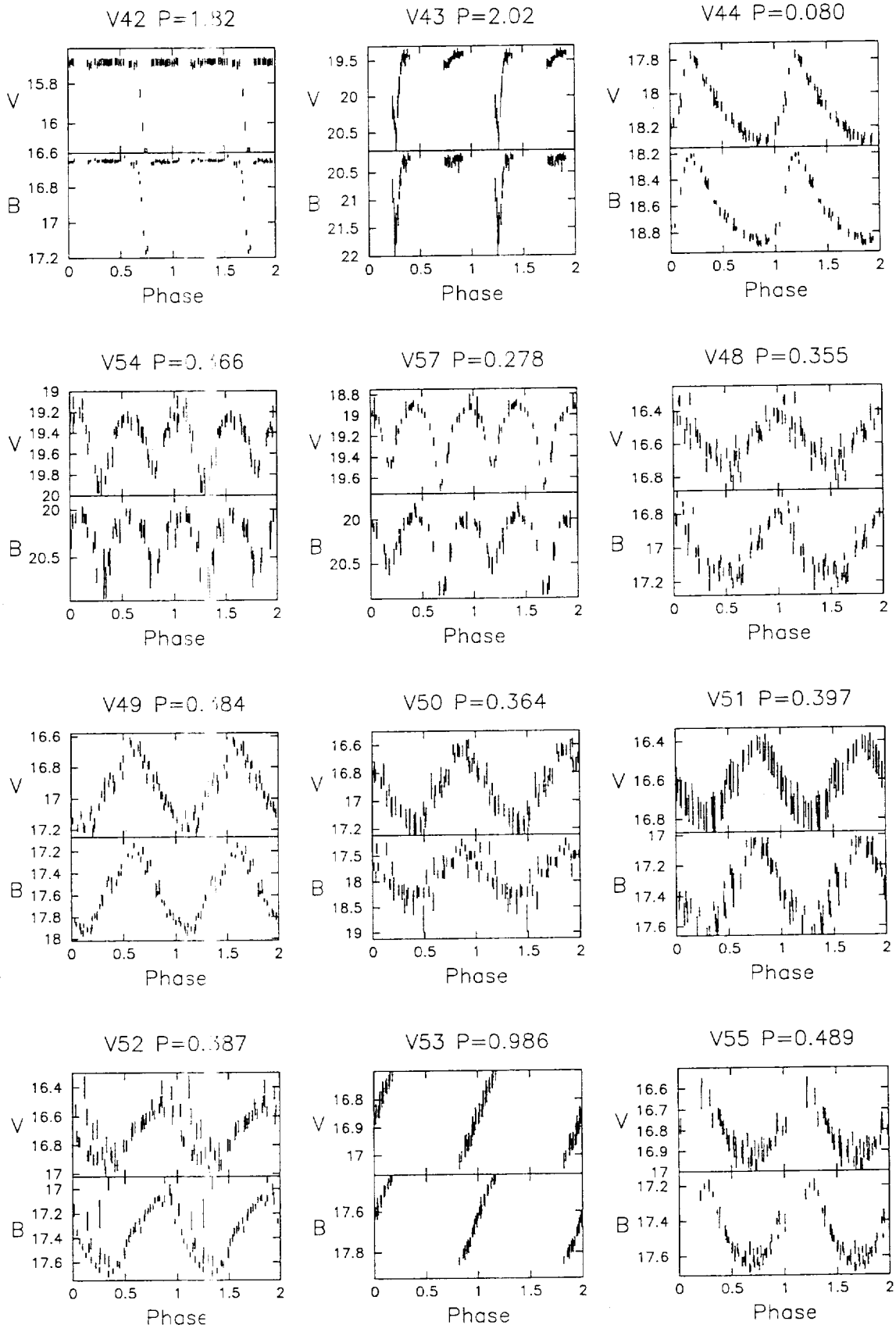
V42 P=1.32
V43 P=2.02
V44 P=0.080
V54 P=0.166
V57 P=0.278
V48 P=0.355
V49 P=0.184
V50 P=0.364
V51 P=0.397
V52 P=0.187
V53 P=0.986
V55 P=0.489
V
B
Phase

Figure 4c

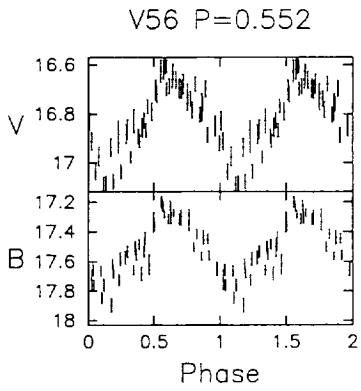

Figure 4d

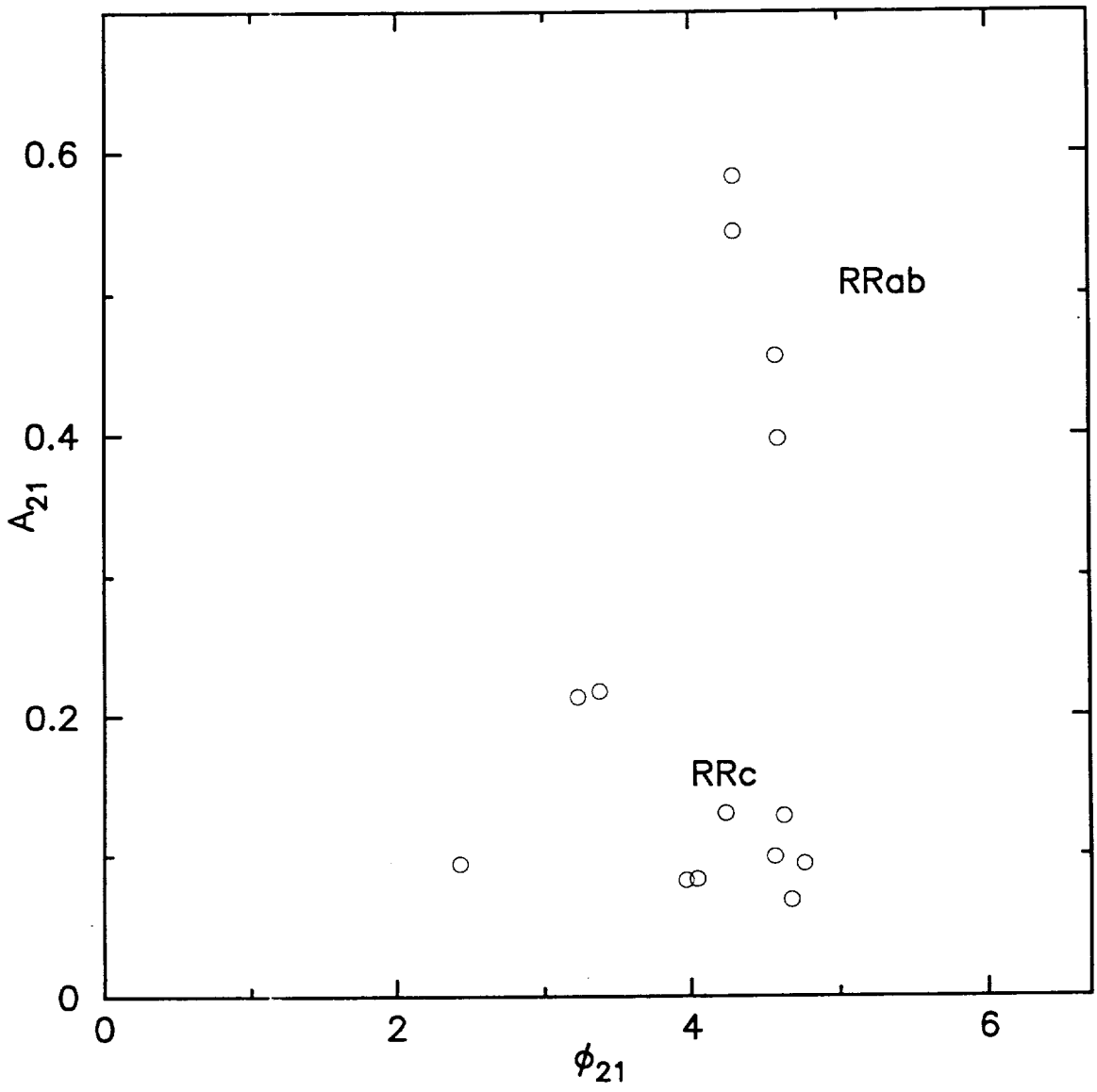

Figure 5

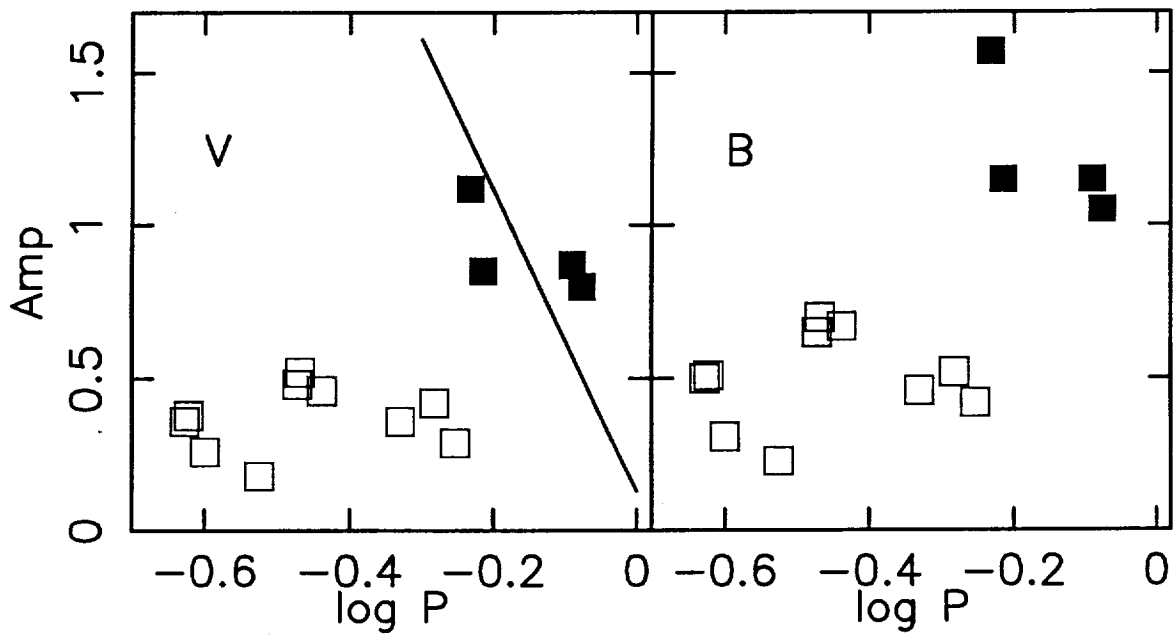

Figure 6

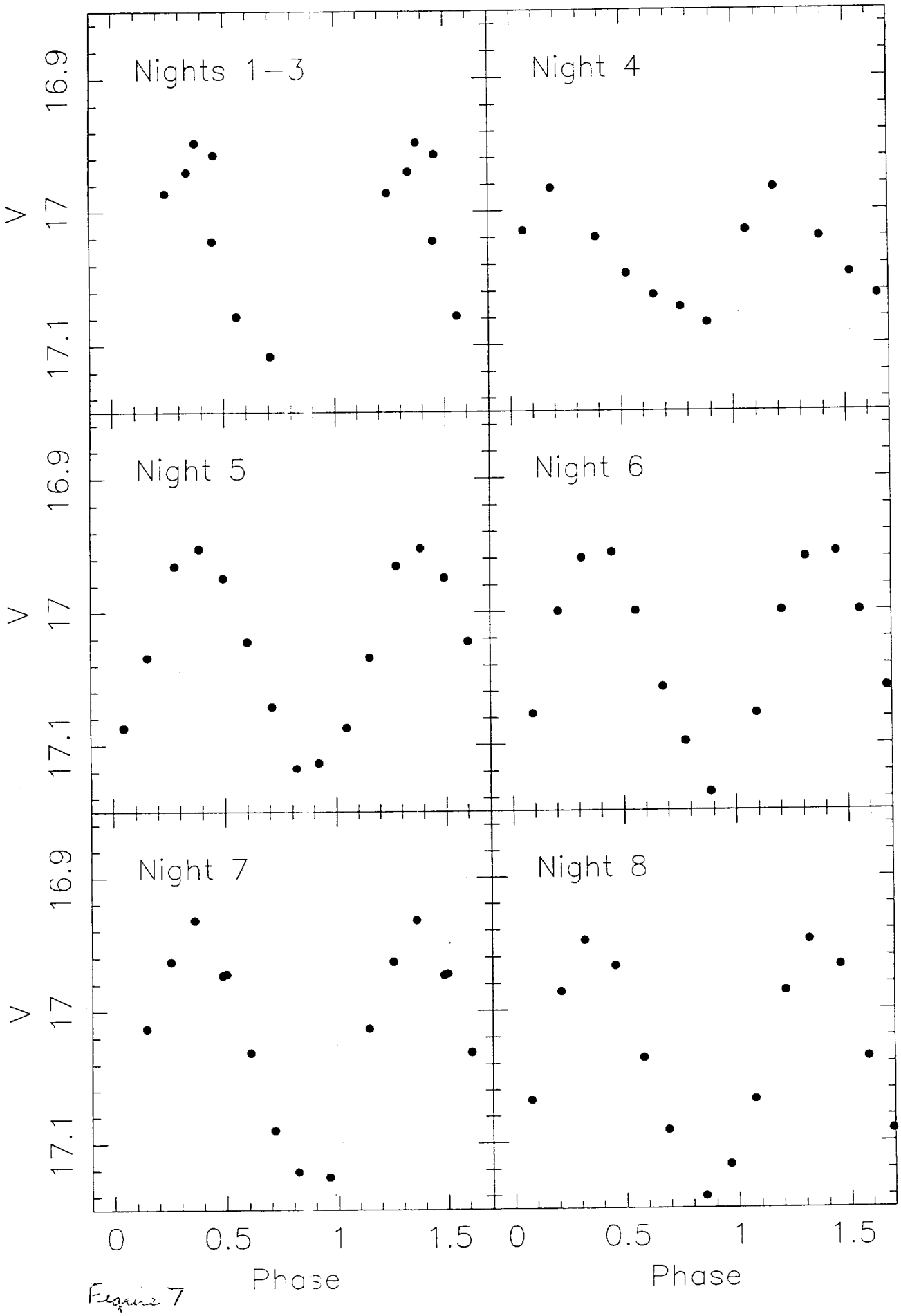
Nights 1–3
Night 4
Night 5
Night 6
Night 7
Night 8
V
16.9
17
17.1
0
0.5
1
1.5
Phase

Figure 7

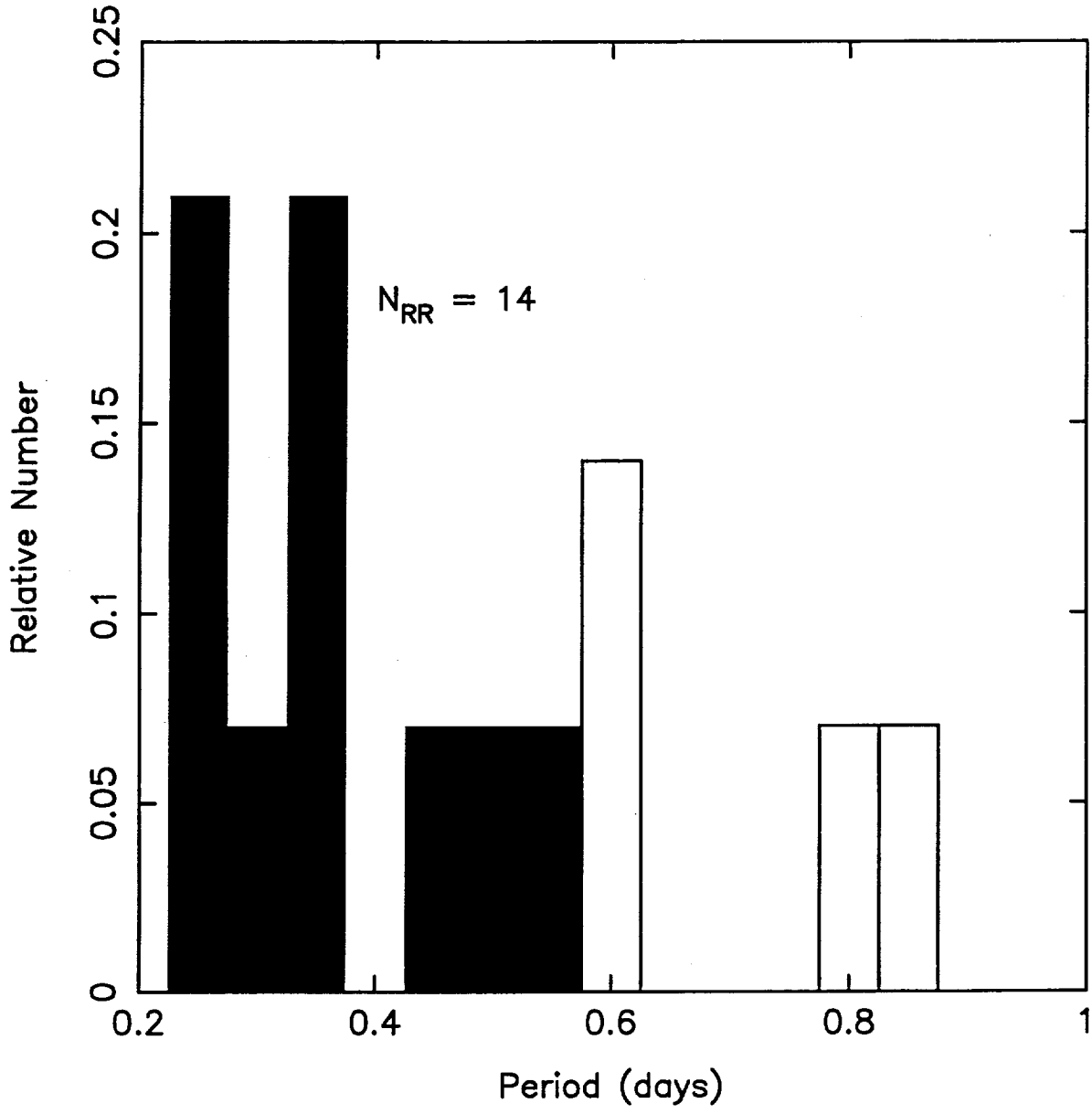
Relative Number
0
0.05
0.1
0.15
0.2
0.25
N_{RR} = 14
0.2
0.4
0.6
0.8
1
Period (days)

Figure 8

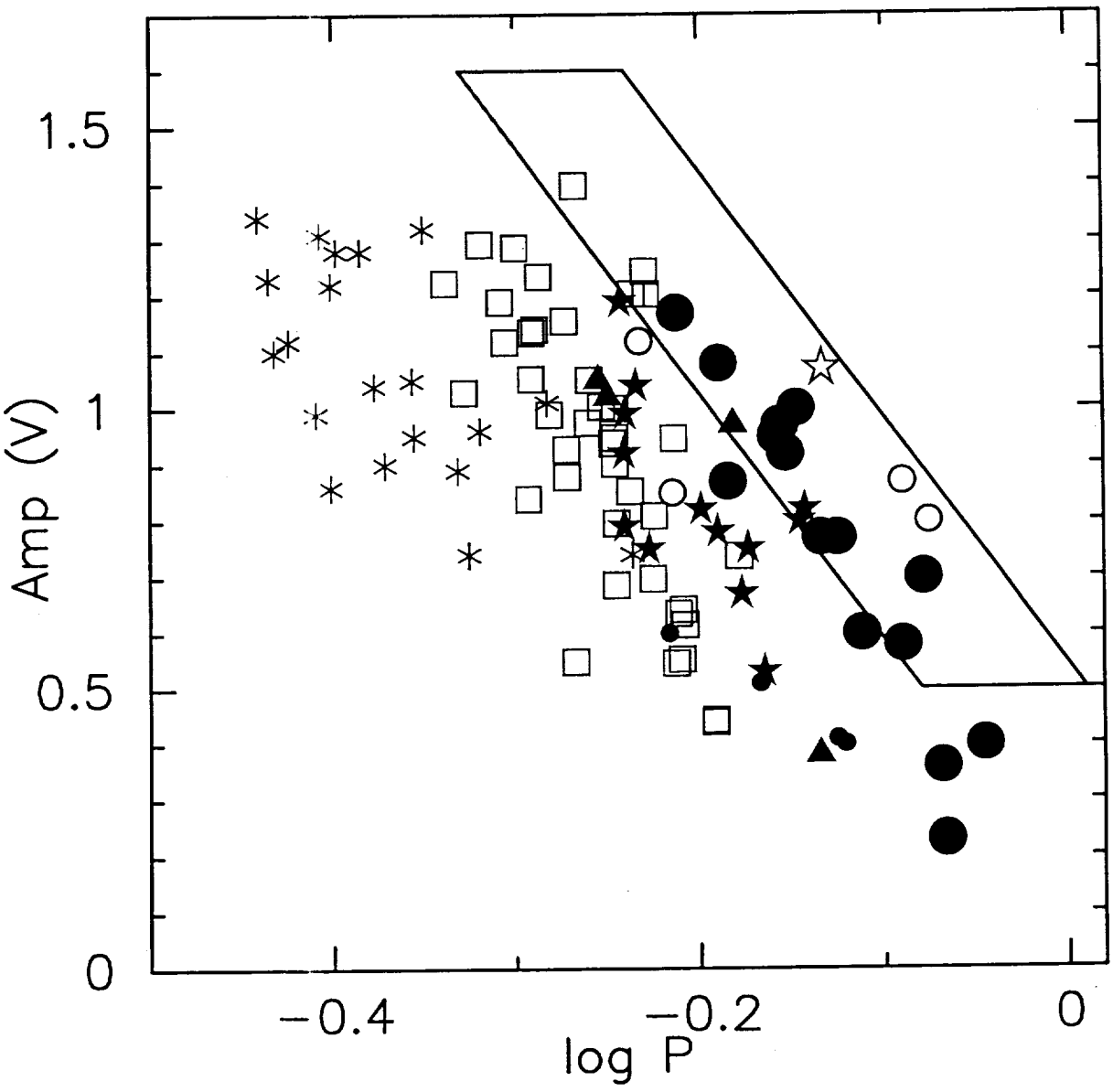

Figure 9

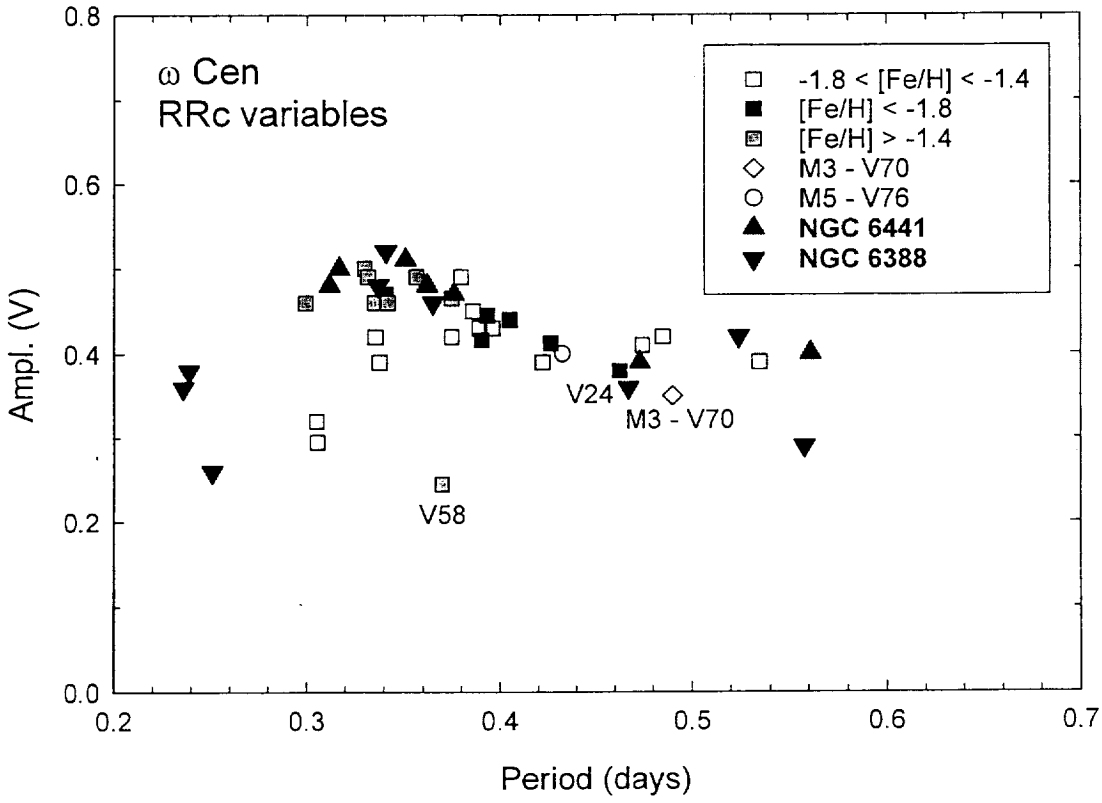
ω Cen
RRc variables
-1.8 < [Fe/H] < -1.4
[Fe/H] < -1.8
[Fe/H] > -1.4
M3 - V70
M5 - V76
NGC 6441
NGC 6388
V24
M3 - V70
V58
Ampl. (V)
Period (days)
0.0
0.2
0.4
0.6
0.8
0.2
0.3
0.4
0.5
0.6
0.7

Figure 10

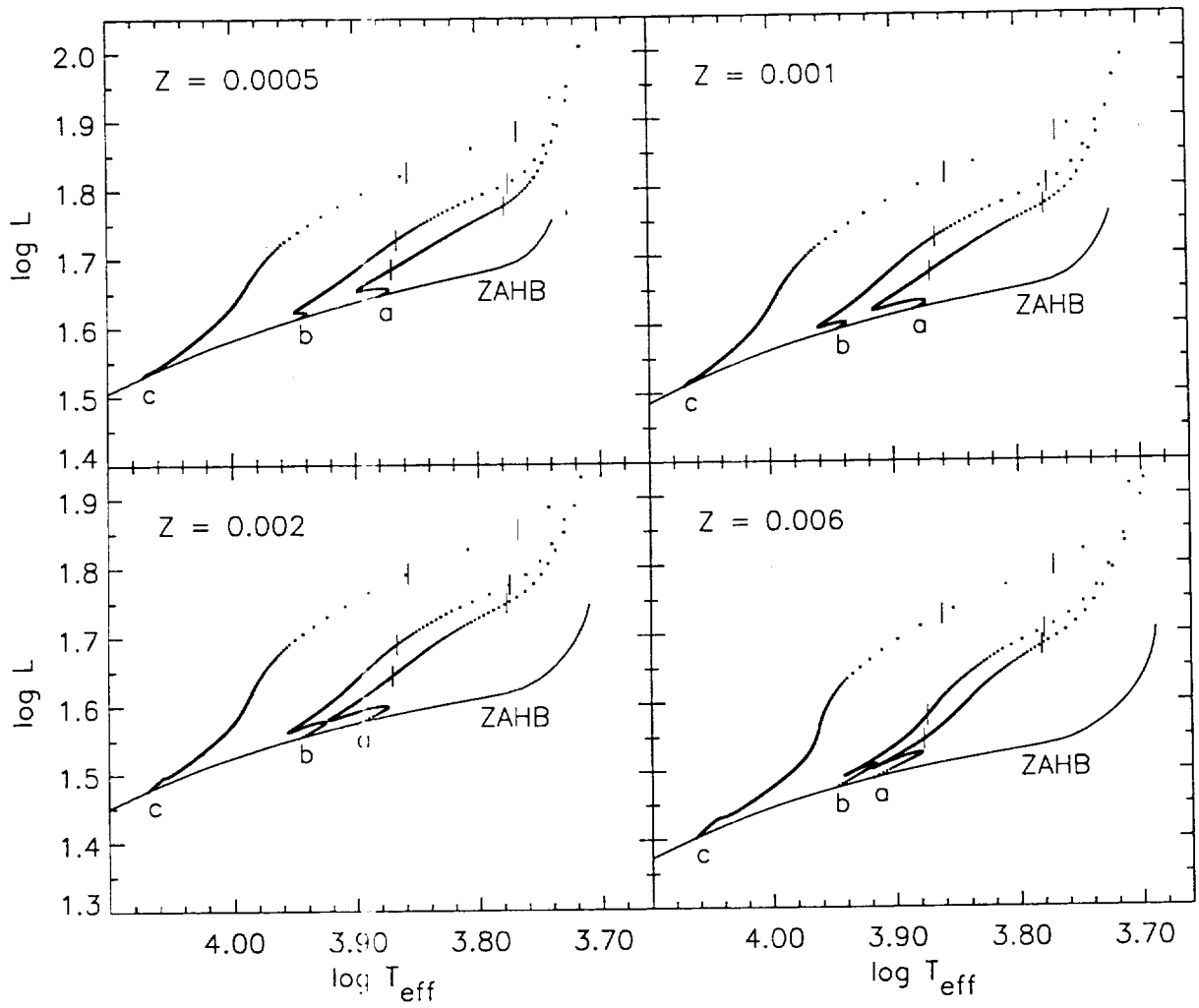
Z = 0.0005
Z = 0.001
Z = 0.002
Z = 0.006
ZAHB
a
b
c
log L
log T_{eff}
2.0
1.9
1.8
1.7
1.6
1.5
1.4
1.3
4.00
3.90
3.80
3.70

Figure 11

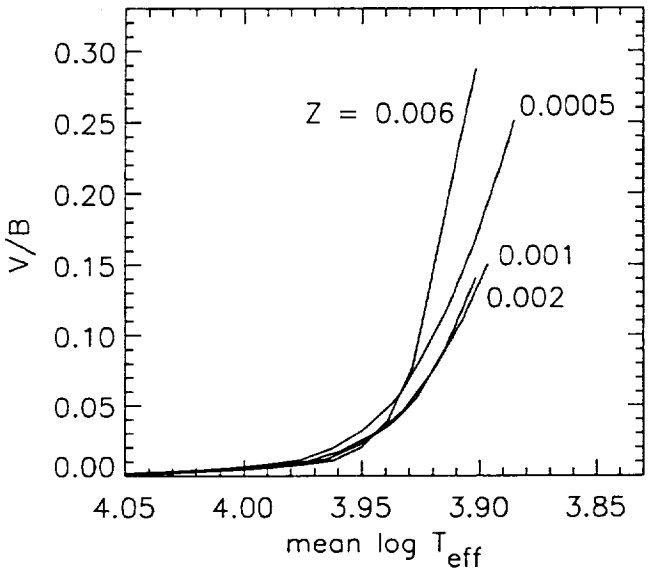
0.30
0.25
0.20
0.15
0.10
0.05
0.00
V/B
Z = 0.006
0.0005
0.001
0.002
4.05
4.00
3.95
3.90
3.85
mean log T_{eff}

Figure 12

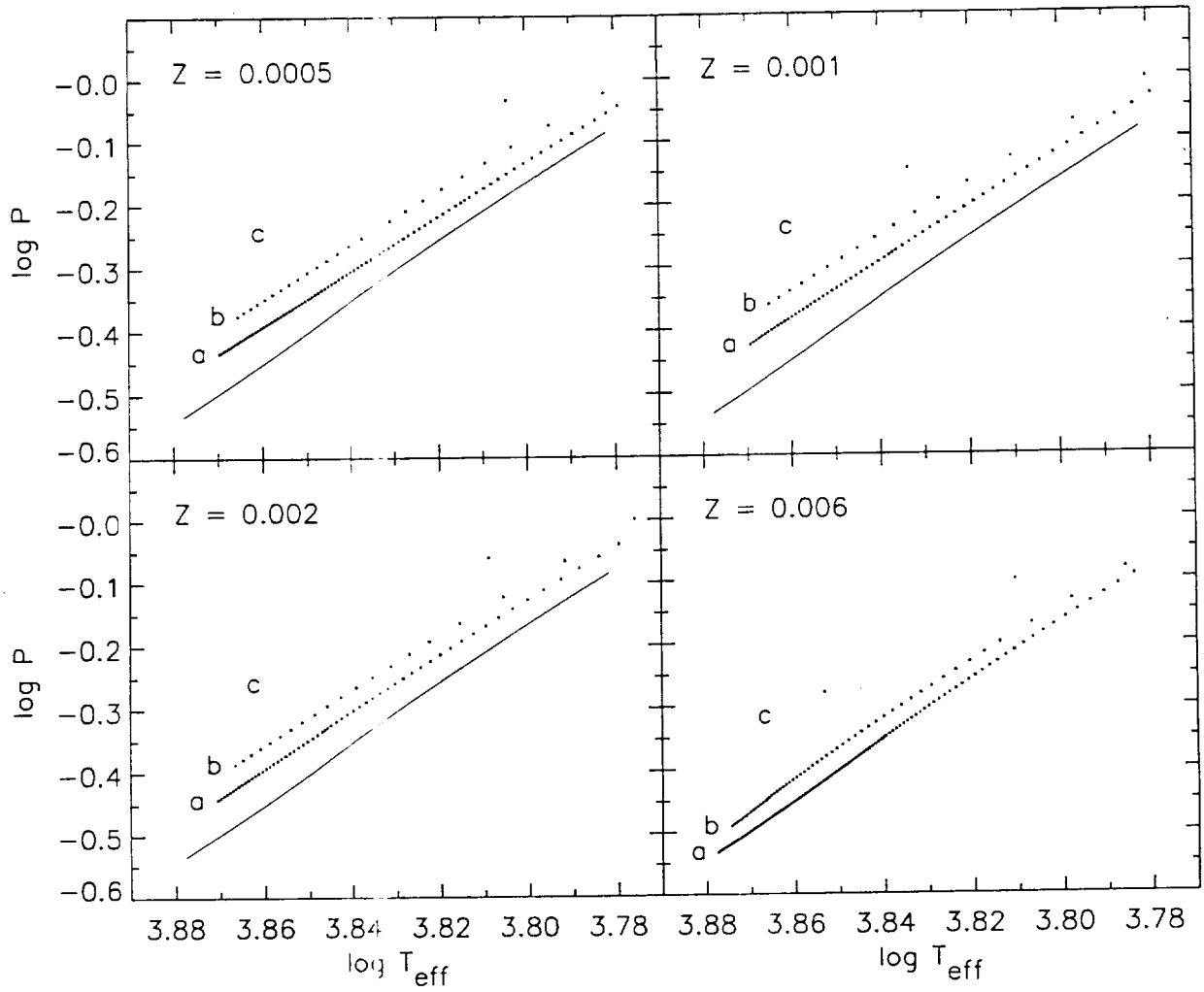
Z = 0.0005
Z = 0.001
Z = 0.002
Z = 0.006
a
b
c
log P
−0.0
−0.1
−0.2
−0.3
−0.4
−0.5
−0.6
3.88 3.86 3.84 3.82 3.80 3.78
log T_{eff}

Figure 13

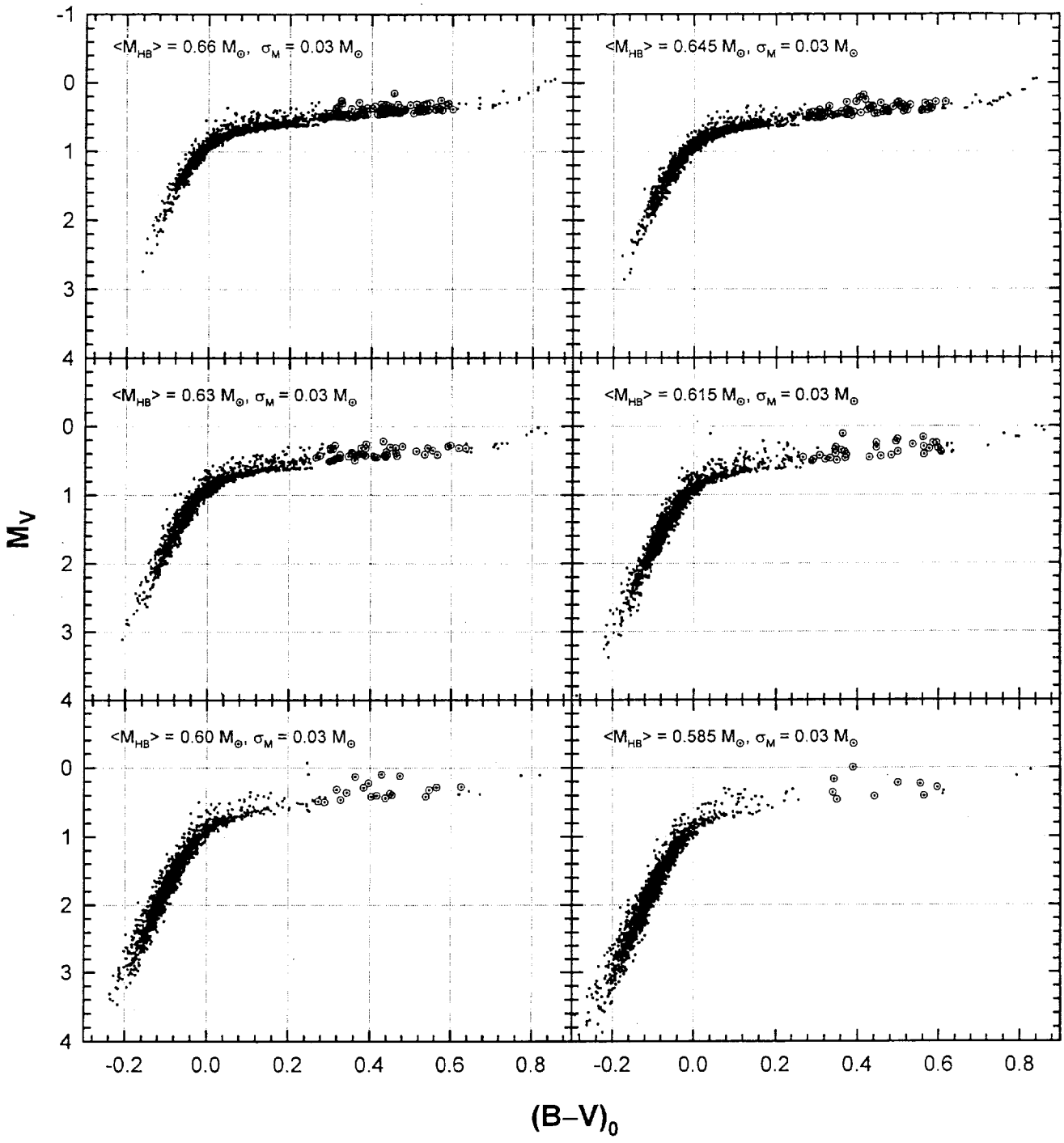
<M_HB> = 0.66 M⊙, σ_M = 0.03 M⊙
<M_HB> = 0.645 M⊙, σ_M = 0.03 M⊙
<M_HB> = 0.63 M⊙, σ_M = 0.03 M⊙
<M_HB> = 0.615 M⊙, σ_M = 0.03 M⊙
<M_HB> = 0.60 M⊙, σ_M = 0.03 M⊙
<M_HB> = 0.585 M⊙, σ_M = 0.03 M⊙
M_V
(B–V)_0
-1
0
1
2
3
4
-0.2
0.0
0.2
0.4
0.6
0.8

Figure 14

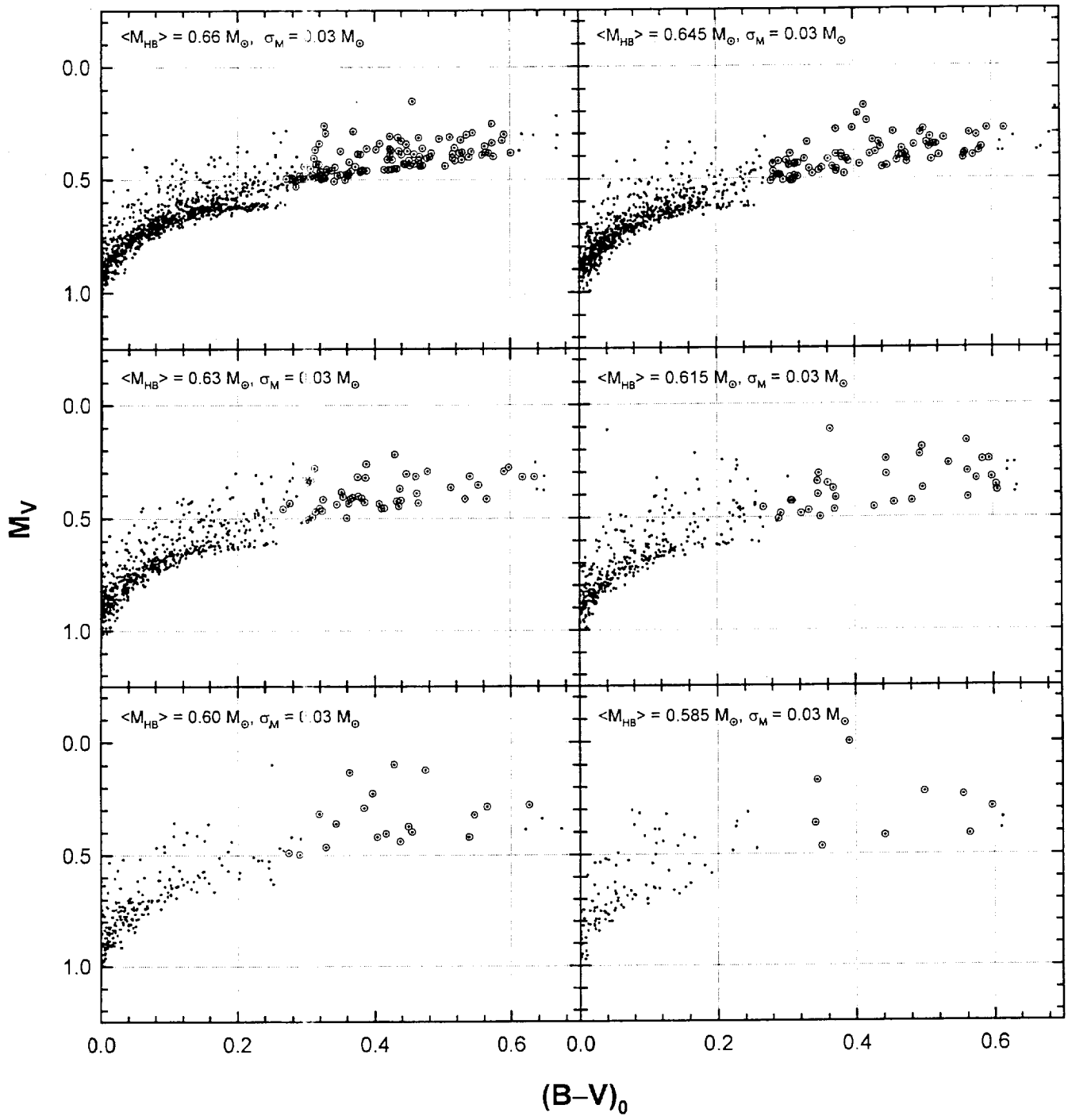
<M_HB> = 0.66 M⊙, σ_M = 0.03 M⊙
<M_HB> = 0.645 M⊙, σ_M = 0.03 M⊙
<M_HB> = 0.63 M⊙, σ_M = 0.03 M⊙
<M_HB> = 0.615 M⊙, σ_M = 0.03 M⊙
<M_HB> = 0.60 M⊙, σ_M = 0.03 M⊙
<M_HB> = 0.585 M⊙, σ_M = 0.03 M⊙
M_V
(B–V)_0
0.0
0.5
1.0
0.2
0.4
0.6

Figure 15

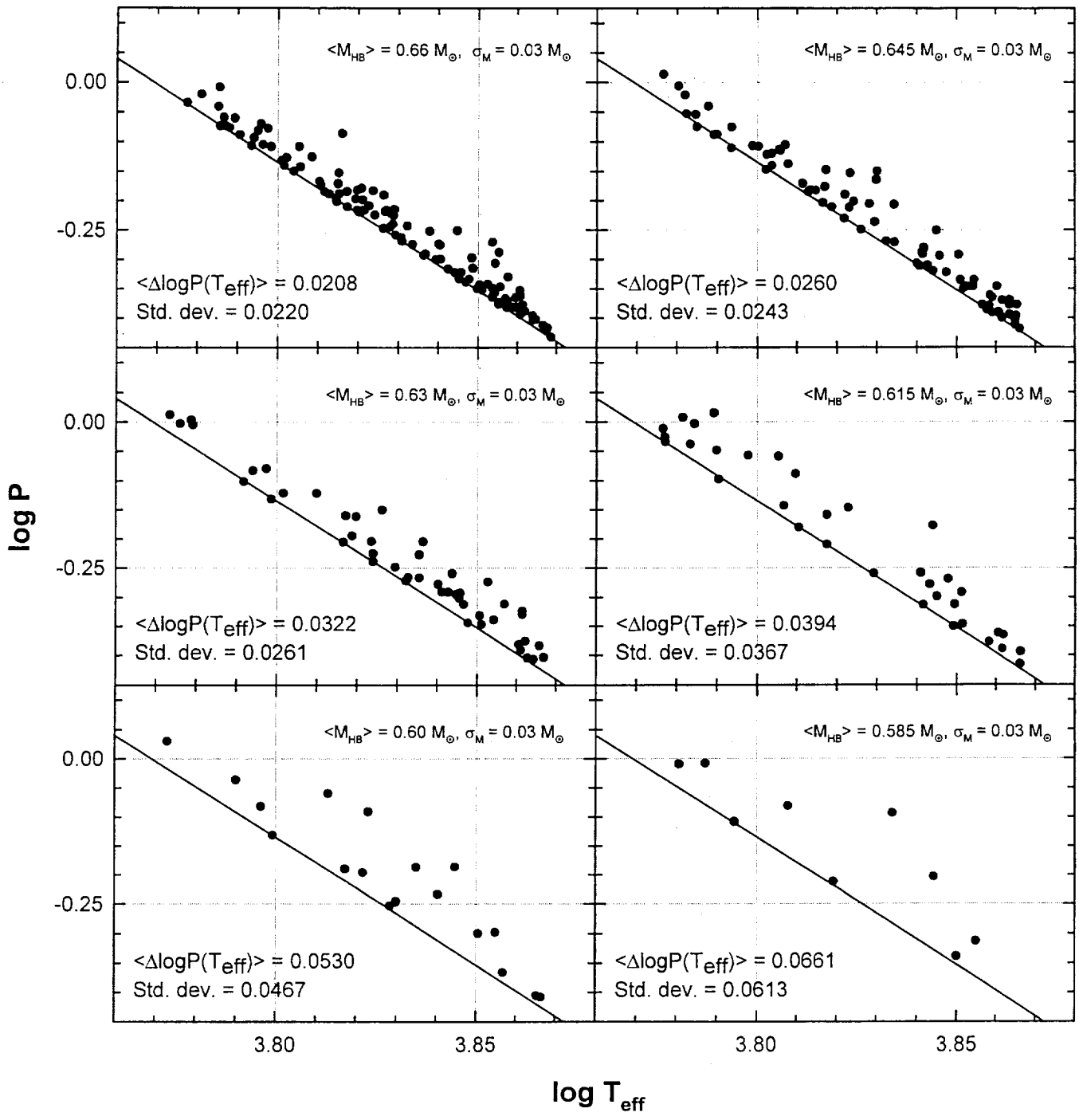
<M_HB> = 0.66 M⊙, σ_M = 0.03 M⊙
<ΔlogP(T_eff)> = 0.0208
Std. dev. = 0.0220
<M_HB> = 0.645 M⊙, σ_M = 0.03 M⊙
<ΔlogP(T_eff)> = 0.0260
Std. dev. = 0.0243
<M_HB> = 0.63 M⊙, σ_M = 0.03 M⊙
<ΔlogP(T_eff)> = 0.0322
Std. dev. = 0.0261
<M_HB> = 0.615 M⊙, σ_M = 0.03 M⊙
<ΔlogP(T_eff)> = 0.0394
Std. dev. = 0.0367
<M_HB> = 0.60 M⊙, σ_M = 0.03 M⊙
<ΔlogP(T_eff)> = 0.0530
Std. dev. = 0.0467
<M_HB> = 0.585 M⊙, σ_M = 0.03 M⊙
<ΔlogP(T_eff)> = 0.0661
Std. dev. = 0.0613
0.00
-0.25
3.80
3.85
log P
log T_eff

Figure 16